RESEARCH ARTICLE

INTERNATIONAL RESEARCH JOURNAL OF MULTIDISCIPLINARY TECHNOVATION

Asian Research Association

DOI: 10.54392/irjmt2561

A Unified Model for Estimation of Reference Evapotranspiration Using an Assembly of Ensemble Learners Coupled with Swarm Intelligence Optimizers

Gouravmoy Banerjee [a], Uditendu Sarkar [b], Indrajit Ghosh [c,*]

[a] Eklavya Model Residential School, Swayem, Namok, Mangan, 737116, Sikkim, India

[b] National Informatics Centre, Ministry of Electronics & Information Technology, Government of India, West Bengal State Centre, Ground Floor, Vidyut Bhawan, DJ Block, Sector II, Saltlake, Kolkata, 700091, West Bengal, India.

[c] Department of Computer Science, Ananda Chandra College, Jalpaiguri, 735101, West Bengal, India.

* Corresponding Author Email: ighosh2002@gmail.com

DOI: https://doi.org/10.54392/irjmt2561

Received: 22-12-2024; Revised: 17-09-2025; Accepted: 05-09-2025; Published: 14-10-2025

Abstract: Several machine learning models and their ensembles have been suggested for reference evapotranspiration (ET_0) modeling at different climatic regions. Researchers reported that optimizing model hyperparameters using an intelligent algorithm significantly improves the performance of such models. However, ensemble models hybridized with hyperparameter optimizers have hardly been applied for the precise estimation of ET_0 worldwide. The current research is devoted to designing sixteen hybrid versions of four ensemble models, alternatively coupled with four popular swarm intelligence optimization algorithms and finding the best-fit model against different input combinations of available climatic parameters for the groundwater-stressed region of North Bengal, India. The performances of four ensemble models and their sixteen hybrid versions were compared in terms of four well-recognized statistical metrics: the coefficient of determination (R^2), Nash-Sutcliffe efficiency (*NSE*), root mean squared error (*RMSE*), and mean absolute error (*MAE*). Experimental results depicted that in nearly 92% of cases, the hybrid versions outperformed the primary ensemble models, irrespective of the available climatic parameters. In most cases, the ensemble models hybridized with the whale optimization algorithm (WOA) produced the highest estimation accuracy, followed by the sailfish optimizer (SFO). Solar radiation was also found to be the most significant climatic parameter for estimating ET_0 in this region.

Keywords: Reference Evapotranspiration, Ensemble Learners, Unified Model, Swarm Intelligence Optimization Algorithms.

1. Introduction

For precise estimation of crop water requirements, intelligent irrigation scheduling, and regional water resource management, reference evapotranspiration (ET_0) has great significance [1, 2]. The existing models for estimating ET_0 are generally categorized into two classes: empirical models and machine learning-based simulation techniques [3]. Several empirical models were suggested [4] that include the Hargreaves-Samani model [5], Priestley-Taylor model [6], Irmak model [7], Makkink model [8], Penman-Monteith (FAO-56 PM) model [9], etc. Each empirical model computes ET_0 using a mathematical equation involving one or more meteorological parameters as inputs. Out of these models, the FAO-56PM model has been recommended by the Food and Agriculture Organization (FAO) as the most standard method to provide a precise estimation of ET_0 [10, 11]. This method is used to validate other models due to its good accuracy [12-14]. However, its application requires a significant amount of meteorological data, which may not be available in rural locations, particularly in developing countries [15]. It becomes a significant flagging in ET_0 estimation using FAO-56PM equation [16]. Furthermore, the estimation of reference evapotranspiration (ET_0) is a nonlinear regression problem, owing to the inherent functional interdependence between input and target variables [17]. The empirical models cannot signify all nonlinear regression processes to provide high estimation accuracy [18, 19].

To overcome the limitations of the empirical models, several machine learning methods were successfully applied to estimate ET_0 with limited inputs when the complete set of meteorological data is hardly available. Another advantage of such machine learners is that they provide more straightforward solutions for

nonlinear multivariable problems and require no prior knowledge about internal functional processes [20]. Over the years, several machine learning methods have been widely applied to design numerous models for estimating ET_0 worldwide [21, 22]. The techniques used to design such models include conventional fuzzy logic [23, 24], artificial neural networks [25-28], decision trees [29, 30], k-nearest neighbor [30, 31], support vector machines [32-34], and other hybrid approaches like adaptive neuro-fuzzy inference system (ANFIS) [35, 36]. Numerous studies have demonstrated that machine learning (ML) algorithms consistently outperform conventional empirical models in estimating reference evapotranspiration (ET_0) due to their enhanced ability to capture complex, nonlinear relationships within meteorological datasets [19, 37-41]. However, these learners have significant limitations, such as determining parameters in the learning algorithms, overfitting of training data, etc. [42].

For better estimation of ET_0, several evolutionary computing (EC) approaches, such as genetic programming (GP) and gene expression programming (GEP) based on genetic algorithm (GA), were suggested. A remarkable review of such systems is available [15]. Most studies reported the limitation in the predictability of EC models using fewer meteorological parameters as inputs.

As an alternative, several ensemble learners were proposed for ET_0 modeling. An ensemble learner is an integration of multiple single learners that provides a more accurate and reliable estimate than a single learner [43]. For better estimation accuracy, model stability, and efficiency, four boosted tree-based ensemble learners, Gradient boosted machines (GBM) [3,17,44], Light gradient-boosted machine (LGB) [3,17,45-48], Extreme gradient boosted machine (XGB) [3,45-48], and Categorical boosting machine (CAT) [3,17, 48-49] are nowadays very well-recognized to estimate ET_0 worldwide.

Though these ensemble learners achieved an acceptable accuracy for estimating ET_0 [3, 17, 44-49], there is an opportunity for further improvement of these models using hyperparameter optimization. Hyperparameters are the structural parameters of a learner, such as the number of estimators, learning rate, number of leaf nodes, etc. The performance of a model depends on properly tuning these hyperparameters [50]. An appropriate tuning of these hyperparameters leads to better performance of a learner with less convergence time [51]. It is evident that instead of a trial-and-error method, hyperparameter optimization using a metaheuristic algorithm significantly improves the performance of a learner and makes it efficient [51]. In recent years, many optimizers based on nature-inspired algorithms have been proposed in the literature to solve various problems [52, 53]. Among them, optimizers based on Swarm intelligence (SI) have been widely adopted to solve problems in most cases (48.54%) [53]. Swarm Intelligence (SI) refers to the emergent collective intelligence exhibited by decentralized, self-organized systems of multiple agents, whose interactions are governed by biologically inspired behavioral rules observed in animal societies like aquatic species, insect colonies, terrestrial herds, and avian flocks. This distributed problem-solving capability enables SI systems to efficiently address complex optimization tasks. Some popular variants of the SI optimizers, such as the Grey wolf optimizer (GWO) [54], Sailfish optimizer (SFO) [55], Salp swarm optimizer (SSO) [56], and Whale optimizer (WOA) [57] are now extensively appreciated by the researchers [58].

For better estimation of ET_0, only a few studies used machine learners coupled with optimization techniques. Quej *et al*. [59] suggested an SVM model optimized using a genetic algorithm (GA), Adib *et al*. [60] used a GA to optimize an ANN model in Iran, Akiner and Ghasri [61] coupled snake optimization with ANFIS models, Tao *et al*. [62] applied a fuzzy model with a firefly optimizer, and Zhao *et al*. [63] used Bayesian optimization (BO) with an Extreme Gradient Boosting Machine (XGB) for estimating ET_0. Elbeltagi *et al*. [64] developed a novel model for predicting ET_0 using the Artificial Bee Colony optimization coupled with ANN in Egypt.

Several researchers reported that instead of a single learner, ensemble learners coupled with hyperparameter optimizers produce better results with less or insufficient data [63, 65, 66]. However, ensemble learners coupled with such optimizers have hardly been reported for ET_0 modeling. Yan *et al*. [66] proposed an XGB model coupled with the whale optimizer (WOA) for estimating ET_0 in China. Han *et al*. [65] suggested another model where XGB was coupled with a Bat optimizer to estimate ET_0 in China's arid and semi-arid regions. Zhao *et al*. [63] estimated reference crop evapotranspiration by optimizing the hyperparameters of GBM using particle swarm optimization (PSO). A significant limitation of these models was that they were designed using only a single ensemble learner coupled with a single optimizer. The proficiency of other learner-optimizer couples was unexplored.

Despite the merits of each optimizer, the “No free lunch” (NFL) theorem demonstrates that a particular learner coupled with a single optimizer cannot always provide the best results for all problems [67]. Choosing the best region-specific learner-optimizer pair for alternative combinations of meteorological parameters by the trial-and-error method is cumbersome, time-consuming, and a major challenge for ET_0 modeling. However, for estimating ET_0, no unified model has been suggested that can automatically select the best-fit learner-optimizer pair to achieve the best result. Therefore, the objective of the present study is to suggest a novel architecture to design a unified model

that can automatically select the best learner-optimizer pair from an assembly and, at all times, assure the best possible result for estimating ET_0, irrespective of the climatic regions and the available meteorological parameters.

To validate our proposed model, case studies were conducted in the North Bengal region of West Bengal state in India. The descriptions of the study area, datasets used, model architecture, and performance evaluation strategies are presented in Section 2. Section 3 describes the results and their analysis from different angles of view. Finally, conclusions are summarized in Section 4.

2. Methods

2.1 Study Area

This study region covers eight districts: Alipurduar, Cooch Behar, Jalpaiguri, Darjeeling, Kalimpong, North Dinajpur, South Dinajpur, and Malda, situated in the North Bengal region of West Bengal, India. It is primarily a rural and technologically backward area where more than half of the population depends on agriculture [68]. About 70% of the total geographical area of this region is used for agriculture, out of which only 43% is under irrigation (https://agricoop.nic.in/en/agriculturecontingency/west-bengal). Groundwater is the major source of water supply for irrigation during the rabi cropping season (November to May), in the North Bengal region. The absence of scientific water management techniques has led to suboptimal irrigation practices among farmers, worsening groundwater exploitation. Regional assessments indicate severe water stress in the ground aquifer during the rabi cropping season [69]. This observation motivated us to select the North Bengal region as our study area to validate our model and to deploy it for precisely estimating reference evapotranspiration (ET_0) as a prime factor in efficient irrigation management. It is to be mentioned that no such study has been conducted in this region so far. Figure. 1. shows the geographic location of the study area.

2.2 Datasets Used

The consistent and reliable datasets used in the present study were obtained from the Indian Meteorological Department, the Government of India (https://dsp.imdpune.gov.in/). Five meteorological parameters: daily minimum and maximum temperatures T_{min} and T_{max} (in ºC), relative humidity R_h (%), wind speed W_s (in Kmph) at 2m height, and solar radiation (S_r) were used as inputs. Daily climatic data from January 2014 to August 2022 were collected from three dispersed weather stations, Jalpaiguri, Cooch Behar, and Malda, under different agroclimatic environments. Due to the lack of sophisticated instruments in these three weather stations, directly measured solar radiation (S_r) data were unavailable. Therefore, solar radiation (S_r) was computed using other available functional parameters, latitude, cloud cover, and the Julian date, using the methods proposed by Allen *et al*. [9].

For a better convergence rate of the ensemble models, the values of all the meteorological parameters were normalized to an interval between 0 to 1, using equation 1 as suggested by Wu *et al*.,[3]:

$$I_n = \frac{I_i - I_{min}}{I_{max} - I_{min}} \quad (1)$$

Where I_n is the normalized input value, I_i is the actual input value, I_{max} and I_{min} are the maximum and minimum values of the input variable, respectively.

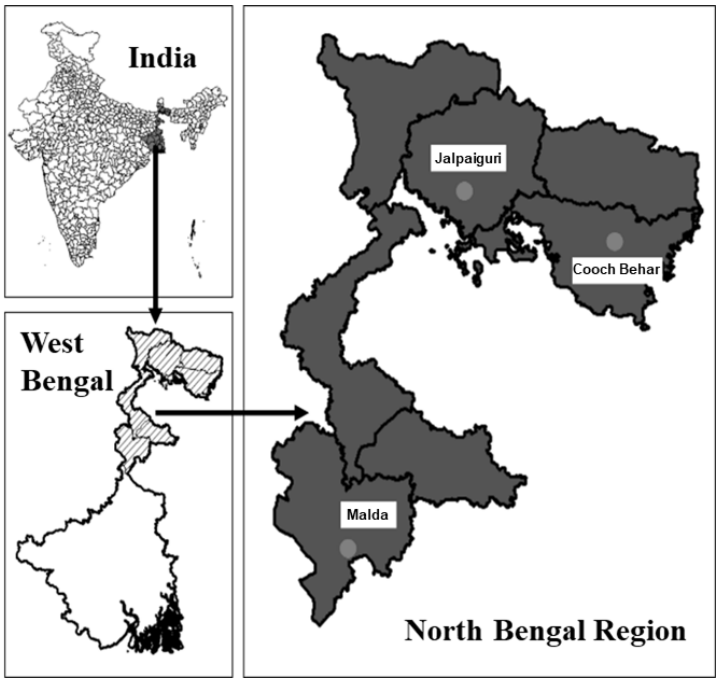

Figure. 1. Geographical area of study

Table 1. Statistical findings of the datasets

			Training Set						Validation Set						Testing Set					
Jalpaiguri	**Latitude: 26.54°N, Altitude:89m**	**Total Samples 2164**	**01/01/2014-27/9/2017**						**28/09/2017-16/09/2020**						**17/09/2020-31/12/2021**					
			Rh	T_{min}	W_s	R_h	S_r	ET_0	T_{max}	T_{min}	W_s	R_h	S_r	ET_0	T_{max}	T_{min}	W_s	R_h	S_r	ET_0
		Max.	38.2	28.7	3.2	98.0	29.4	6.2	37.9	28.2	2.1	97.3	29.0	5.8	37.2	28.1	5.7	97.5	29.4	6.3
		Min.	14.1	6.2	0.0	41.5	6.2	1.0	14.8	7.3	0.0	38.0	6.3	1.0	15.0	6.9	0.0	42.5	6.2	1.0
		Avg.	30.4	20.0	0.6	77.3	17.2	3.3	29.8	19.4	0.3	74.2	16.9	3.1	30.9	19.7	0.4	74.0	16.6	3.1
		Std. Dev.	4.0	5.8	0.5	10.0	4.3	1.1	3.9	5.6	0.3	11.9	4.0	1.0	3.6	5.6	0.5	11.2	4.6	1.1
		Kurt.	0.8	-1.1	2.7	0.2	0.0	-0.5	1.0	-1.0	4.0	-0.4	0.1	-0.5	0.9	-1.2	22.8	-0.4	0.4	0.4
		Skew.	-0.9	-0.5	1.6	-0.6	0.4	0.3	-0.9	-0.4	1.8	-0.4	0.4	0.2	-0.8	-0.4	3.4	-0.2	0.6	0.8
Cooch Behar	**Latitude: 26.32°N, Altitude:48m**	**Total Samples 2343**	**Training Set**						**Validation Set**						**Testing Set**					
			01/01/2014-12/08/2017						**13/09/2017-29/09/2017**						**29/09/2020-31/12/2021**					
			T_{max}	T_{min}	W_s	R_h	S_r	ET_0	T_{max}	T_{min}	W_s	R_h	S_r	ET_0	T_{max}	T_{min}	W_s	R_h	S_r	ET_0
		Max.	38.9	27.8	6.1	99.0	29.4	6.7	38.2	27.6	3.3	98.0	28.8	6.1	37.7	28.3	24.4	98.3	29.0	7.4
		Min.	14.4	4.7	0.0	37.5	6.6	1.1	15.4	3.9	0.0	38.5	7.3	1.3	14.7	5.6	0.0	35.8	6.3	1.2
		Avg.	30.4	19.2	0.9	76.0	16.7	3.3	29.4	17.1	0.9	74.6	17.1	3.2	29.6	18.4	1.0	72.3	16.6	3.2
		Std. Dev.	3.7	6.0	0.6	11.3	3.9	1.0	3.8	6.7	0.4	9.4	4.2	1.1	4.0	6.2	1.6	13.2	4.6	1.2
		Kurt.	0.9	-1.1	10.1	0.0	0.1	-0.3	0.5	-1.3	4.3	0.0	-0.2	-0.9	0.3	-1.2	174.7	-0.4	0.2	0.2
		Skew.	-0.8	-0.5	2.1	-0.5	0.4	0.3	-0.5	0.0	1.4	-0.2	0.3	0.3	-0.5	-0.3	12.5	-0.1	0.7	0.8
Malda	**Latitude: 24.99°N, Altitude:17m**	**Total Samples 2126**	**Training Set**						**Validation Set**						**Testing Set**					
			01/01/2014-29/08/2017						**30/08/2017-28/09/2020**						**29/09/2020-31/12/2021**					
			T_{max}	T_{min}	W_s	R_h	S_r	ET_0	T_{max}	T_{min}	W_s	R_h	S_r	ET_0	T_{max}	T_{min}	W_s	R_h	S_r	ET_0
		Max.	42.0	32.0	2.2	97.4	29.5	7.3	39.0	30.0	1.9	95.3	27.5	5.7	40.0	30.0	1.9	94.9	27.9	6.4
		Min.	16.0	8.0	0.0	25.5	6.4	1.1	16.0	6.0	0.0	36.0	7.1	1.2	0.0	10.0	0.0	39.8	7.1	1.3
		Avg.	31.3	22.2	0.6	73.0	17.5	3.5	31.3	23.1	0.5	74.2	17.3	3.5	29.8	20.6	0.5	73.9	16.9	3.2
		Std. Dev.	4.8	5.4	0.3	12.4	4.1	1.1	4.3	5.3	0.3	11.4	4.1	1.0	5.1	5.6	0.3	10.7	3.8	1.1
		Kurt.	0.1	-0.8	1.4	1.0	0.1	0.0	1.4	0.6	2.1	0.6	-0.4	-0.6	1.8	-1.2	1.8	0.0	-0.1	-0.5
		Skew.	-0.6	-0.7	0.8	-0.9	0.5	0.5	-1.3	-1.1	1.1	-0.9	0.2	0.0	-0.6	-0.1	1.0	-0.6	0.3	0.6

The normalized (master) datasets were divided into three groups in a 60:20:20 ratio. The first group (60%) was used as a training dataset to train the four ensemble models; the second group (20%) was used as a validation dataset to tune the hyperparameters of each model; and the rest (20%) of the datasets were used as testing datasets to evaluate the performance of the models. The statistical findings of the datasets collected from the three weather stations (Jalpaiguri, Cooch Behar, and Malda) are provided in Table 1.

The training, hyperparameter optimization, and evaluation of each model were conducted using eight distinct input combinations derived from five available meteorological parameters: minimum temperature (T_{min}), maximum temperature (T_{max}), wind speed (W_s), relative humidity (R_h), and solar radiation (S_r). The eight input combinations comprised the following configurations:The eight input combinations are: C_1 = {T_{min}, T_{max}}, C_2 = {T_{min}, T_{max}, W_s}, C_3 = {T_{min}, T_{max}, R_h}, C_4 = {T_{min}, T_{max}, S_r}, C_5 = {T_{min}, T_{max},W_s, R_h}, C_6 = {T_{min},

T_{max},W_s, S_r}, C_7 = {T_{min}, T_{max}, R_h, S_r}, and C_8={T_{min}, T_{max},W_s, R_h, S_r}. For the input combination C_8 = {T_{min}, T_{max}, W_s, R_h, S_r}, the normalized master datasets were directly used as they contained the complete set of all five parameters. For the other seven input combinations (C_1 to C_7), respective subsets of data were mined from the master datasets.

2.3 Reference Values of ET_0

As a widely accepted practice, the ET_0 values calculated using the FAO-56PM method [9] were considered as the reference (target) values of ET_0 for training, validation, and testing of the models [10, 11]. The reference values of ET_0 (ET_{0PM}) (mm d^{-1}) were calculated using the FAO-56PM equation:

$$ET_{0PM} = \frac{0.408\times\Delta\times(R_a-G)+\gamma\times\frac{900}{T+273}\times u_2\times(e_s-e_a)}{\Delta+\gamma\times(1+0.34\times u_2)} \quad (2)$$

Where R_a denotes the net radiation measured in MJ m^{-2} day^{-1},G represents the soil heat flux density measured in MJ m^{-2} day^{-1}),T is the mean daily air temperature measured in C,u_2 corresponds to the wind speed measured at 2 m above the ground surface measured in m s^{-1},e_s and e_a represents the saturation vapor pressure and actual vapor pressure, respectively, measured in kPa,Δ refers to the slope of the vapor pressure curve measured in kPa C^{-1}, and γ stands for the psychrometric constant, which is measured in kPa C^{-1}. All of the parameters used to estimate ET_0 by the FAO-56PM equation are calculated using 24 additional equations from various atmospheric variables, including temperature, humidity, wind speed, etc., [9].

2.4 Model Architecture

Four decision tree-based ensemble learners, GBM, LGB, XGB, and CAT, were chosen as the primary learners for the proposed model, and four swarm intelligence-based optimizers GWO, SFO, SSO, and WOA, were used for hyperparameter optimization. Each of these four primary learners was alternatively coupled with four SI optimizers (GWO, SFO, SSO, and WOA). Considering all possible combinations, a total of sixteen learner-optimizer pairs were designed. The learner assembly was created with the four primary learners and the sixteen learner-optimizer pairs. A total of twenty learners (four primary learners and sixteen learner-optimizer pairs) were used for estimating ET_0 with the location-specific dataset, as presented in Table 2.

The model architecture and general method adopted to couple each primary learner with an optimizer are presented in Figure 2. In the first step, each primary learner was trained with training datasets. The hyperparameters of each trained primary learner were optimized by each of the optimizers using validation datasets to obtain an optimized learner (learner-optimizer pair) in the second step. Finally, the performance evaluator evaluates the performance of each of the twenty learners in the assembly in terms of four performance metrics using the testing datasets and selects the best one to give the output. Each of these primary learners was developed using the standard Python library packages of Scikit-learn. The SI optimizers were coded by the authors using Python.

2.5 Primary Learners

The present study used four tree-based ensemble learners, GBM, LGB, XGB, and CAT, as the primary learners. Each of these primary learners was an ensemble of multiple weak learners (decision tree-based ML models) that used a boosting algorithm for their training. The main principle behind the boosting algorithms is that a collection of weak learners can provide better results than an individual weak learner [70]. These algorithms use an iterative approach to obtain more accurate results by combining the outputs of several weak learners into strong learners [71]. The process starts by creating a learner, and then the next learner corrects the mistakes made by the previous learner to provide better results, and so on. The iterative optimization process continues to generate progressively stronger learners until a predefined convergence criterion is met. Subsequently, the outputs of all constituent learners are aggregated through a weighted average approach to derive the final prediction [72]. Several literatures have been published on the training functions, algorithms, and various applications of these four ensemble models since their first appearances [72-75]. An overview of each of these four primary learners is presented in the following subsections.

2.5.1. Gradient Boosted Machines (GBM)

A gradient boosted machine is a decision tree-based ensemble learner first proposed by Friedman [72]. It is a popular machine-learning algorithm due to its accuracy, efficiency, and interpretability. The gradient refers to the pseudo-residuals or errors made by the individual decision tree learners [76]. In a gradient boosted machine, each learner tree tries to minimize the errors made by its predecessor tree to improve the prediction performance. Each learner is assigned a weight (learning rate) to avoid overfitting. The iterative process of generating new learners continues until a stopping condition (e.g., the maximum number of estimators) is met. The final prediction is obtained by a weighted summation of the predictions made by all the learners in the ensemble.

2.5.2. Extreme Gradient Boosted Machine (XGB)

The Extreme Gradient Boosted Machine is an improved version of the Gradient Boosted Machine [73].

Table 2. Four ensemble models and their sixteen optimized versions

Sl. Nos.	Base models	Optimizers	Optimized versions	Model description
1.	GBM	-----	-----	GBM base model
2.	GBM	GWO	GBM+GWO	GBM coupled with GWO
3.	GBM	SFO	GBM+SFO	GBM coupled with SFO
4.	GBM	SSO	GBM+SSO	GBM coupled with SSO
5.	GBM	WOA	GBM+WOA	GBM coupled with WOA
6.	LGB	-----	----	LGB base model
7.	LGB	GWO	LGB+GWO	LGB coupled with GWO
8.	LGB	SFO	LGB+SFO	LGB coupled with SFO
9.	LGB	SSO	LGB+SSO	LGB coupled with SSO
10.	LGB	WOA	LGB+WOA	LGB coupled with WOA
11.	XGB	-----	----	XGB base model
12.	XGB	GWO	XGB+GWO	XGB coupled with GWO
13.	XGB	SFO	XGB+SFO	XGB coupled with SFO
14.	XGB	SSO	XGB+SSO	XGB coupled with SSO
15.	XGB	WOA	XGB+WOA	XGB coupled with WOA
16.	CAT	-----	----	CAT base model
17.	CAT	GWO	CAT+GWO	CAT coupled with GWO
18.	CAT	SFO	CAT+SFO	CAT coupled with SFO
19.	CAT	SSO	CAT+SSO	CAT coupled with SSO
20.	CAT	WOA	CAT+WOA	CAT coupled with WOA

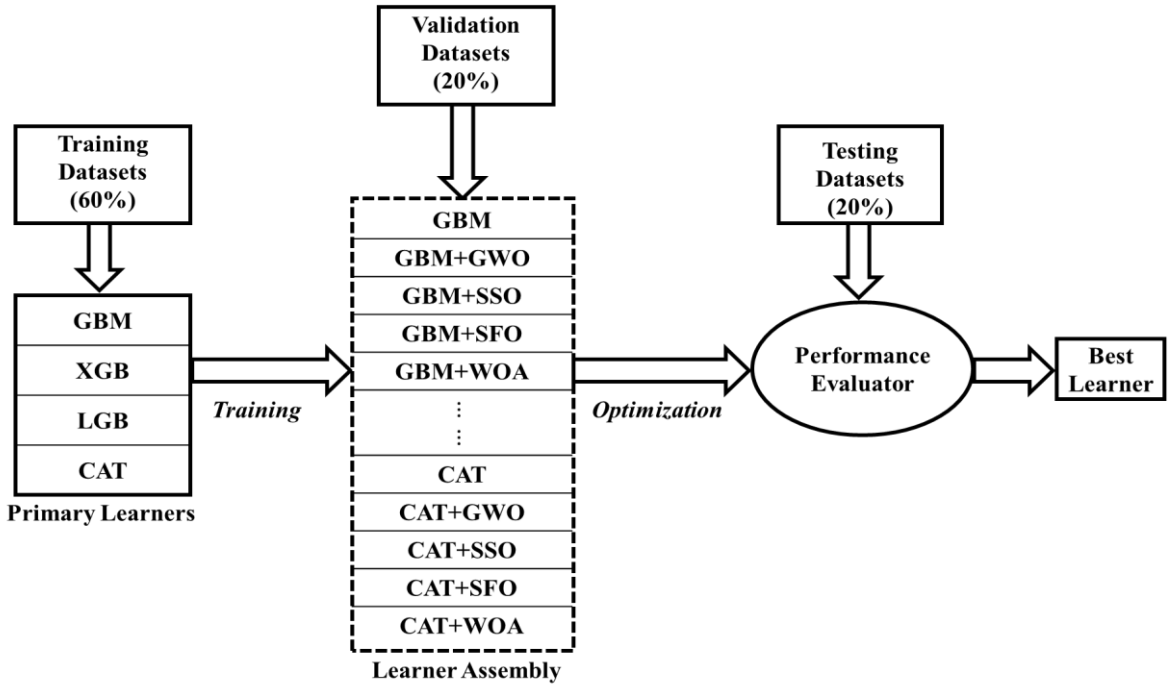

Figure 2. The general architecture of optimizer coupling

The improvement is achieved using a second-order Taylor series expansion of the loss function (or objective function), added with a regularization parameter. The addition of the regularization parameter maintains the bias-variance tradeoff and prevents overfitting, making XGB superior to GBM. The XGB is a fast learner as compared to classical GBM.

2.5.3. Light Gradient Boosted Machines (LGB)

A Light gradient boosted machine learning model was developed by Ke *et al*. [74]. This model has

the advantages of low space requirement, less training time, better accuracy, and the capacity to treat large-scale data. The light gradient boosted model follows depth expansion (leaf-wise) of the consecutive learner trees rather than breadth-wise (level-wise) expansion. For more scalability of the model, it employs two sets of algorithms: Gradient-based One Side Sampling (GOSS) and Exclusive Feature Bundling (EF-B). The GOSS algorithm considers only samples that offer more information gain than a given threshold value, leading to more accuracy. The EF-B algorithm bundles multiple feature sets into a single domain, acting as a dimensionality reduction method. LGB combines the information gains of the left and right subtrees into a single learning function [74, 77].

2.5.4. Categorical Boosted Machines (CAT)

Categorical boosted machines (CAT) or gradient boost with categorical features is an open-source algorithm [75]. This algorithm is based on a target encoding strategy for categorical features employing target-based statistics [78]. The CAT model is capable of integrating multiple features into a single feature following a greedy approach. CAT uses ordered boosting to overcome prediction shifts caused by gradient bias [49]. Unlike the other boosting machines, it considers the same feature-splitting criterion at the same level of the tree, helping to tackle the overfitting problem.

2.6 Model Hyperparameters

Five contributory hyperparameters common to four decision tree-based ensemble learners were selected for optimization. The five hyperparameters were: the *maximum number of trees in the ensemble* (η), *learning rate* (α), *maximum depth of each tree* (λ), the *maximum number of leaf nodes for each tree* (ρ), and the *subsample of the training dataset* (σ) used for training (generating) the trees. Each of these five hyperparameters is very critical in determining the tree size, the number of trees in an ensemble, and the structure of each tree. The η value defines the number of trees to be used in the ensemble model. It is a critical factor that determines the complexity of the learner and is responsible for controlling the boosting quantity [79]. The learning rate α controls the weights to be assigned to each of the weak learners and assigns weightage to each tree based on its accuracy of prediction. It is inversely proportional to the errors in the predictions of each tree. The λ controls the height of each tree, and the hyperparameter ρ regulates the upper bound of the number of terminal nodes in the tree. The σ is another vital tunable hyperparameter, which directly controls the training data used while generating the individual tree. Adjusting this hyperparameter to an optimum value ensures that the learners are not overfit. Thus, an optimizer aims to provide the best model having an optimum number of trees and of optimum size [80]. The range of the values of each of the five hyperparameters is provided in Table 3.

Table 3. Hyperparameters and their range of values

Hyperparameters	Range of values
Maximum number of trees in the ensemble (η)	1-500
Learning rate (α)	0.1-1.0
Maximum depth of each tree (λ)	1-10
Maximum number of leaf nodes for each tree (ρ)	2-10
Subsample of training dataset used for training the trees (σ)	0.1-1.0

2.7 Hyperparameter Optimizer

In most machine learning models, the values of the hyperparameters are set to some predefined values that cannot be adjusted during training. A significant limitation of this approach is that the loss (error) function may get stuck in the local minima. The models do not achieve their full potential in such cases and produce comparatively poor accuracy [81]. The performance of an ML model depends on the proper tuning of these hyperparameters [50]. Therefore, obtaining the best values of the hyperparameters is essential so that the ML model can achieve its full potential with less convergence time [51].

Several hyperparameter optimizers have been suggested that use different algorithms, such as Bayesian optimization [82], gridded search [83], nature-inspired optimization (NIO), cross-validation, gradient descent, etc., [2]. The optimizers using nature-inspired algorithms are very popular in recent times [52] and perform better than others [84]. Among them, swarm intelligence (SI) based optimizers are the most prevalent for solving optimization problems [53].

In our present study, four widely applied SI optimizers, Grey wolf optimizer (GWO) [54], Sailfish optimizer (SFO) [55], Salp swarm optimizer (SSO) [56], and Whale optimizer (WOA) [57] were selected to optimize four primary learners. The selection was based on three criteria, current popularity of the optimizer, recency (year of publication) of the optimizer, and occurrence of being more accurate (champion), as suggested by Li *et al*. [58]. The optimization functions, algorithms, and other details of these four optimizers are available in Mirjalili *et al*.,(2014) [54], Shadravan *et al*. [55], Mirjalili *et al*. (2017) [56], and Mirjalili and Lewis [57].

2.7.1. Grey Wolf Optimizer (GWO)

The GWO is a multi-elite strategy-based optimizer inspired by the hunting mechanism of the grey

wolf (*Canis lupus*) pack [54]. There are divisions of social hierarchy among the wolves, mainly *alpha*, *beta*, *delta,* and *omega,* each with its own assigned job. The *alphas* are considered the responsible leaders to make decisions on every aspect of the entire pack. The *betas* are second in command and help the *alphas* in decision-making; *while dominating the omegas, deltas* are under the *alphas* and *betas*. The *omegas* are the lowest in the social hierarchy, carry out daily menial jobs, and are considered scapegoats. Each member of this hierarchy represents a solution to a given optimization problem. The solution hierarchy follows a descending order of accuracy, with *alpha* representing the best solution, followed by suboptimal solutions *beta* and *delta*, while all remaining solutions with lower accuracy fall under *omega*.

2.7.2. Sailfish Optimizer (SFO)

The SFO is another swarm intelligence-based optimizer [55]. Contrary to GWO, this algorithm is a single-elite-based algorithm with only one best solution. This algorithm is inspired by the sailfish (*Istiophorus platypterus*) hunting style of sardine prey (*Sardinella aurita*). This algorithm considers two fish categories: the sailfish and the sardine distributed across the search space. The sailfish population searches for the nearest sardine and injures it. This injured sardine is the best solution among the sardine population. If the sardines in the algorithm can provide a better solution than the current elite sailfish, the elite sailfish will take over the sardine's position and replace it. That is, the value of the elite will be initialized by that of the sardine providing a better solution.

2.7.3. Salp Swarm Optimizer (SSO)

SSO is also a single elite swarm intelligence-based optimizer inspired by the foraging method of salps [56]. The algorithm was developed in a manner that mathematically tries to represent the hunting techniques of the salps. The salps hunt for food by making a Fibonacci-type structure where the origin point is the position of the leader (best position). The position of the other salps gets updated depending on the leader's current position.

2.7.4. Whale Optimizer (WOA)

The WOA [57] is based on the scavenging mechanism of humpback whales. These whales use a technique called the bubble net feeding method for hunting fish. This is also a single-elite NIO, as only one whale gives the best solution. The bubble net feeding method is implemented using two separate strategies, mainly encircling the prey and then shrinking the circle towards it and a spiral attack [58].

2.8 Performance Evaluation

The assessment of the performance of a machine learner using a single metric may lead to a unidirectional interpretation of the results. Evaluating the performance of a learner using multiple metrics is used to ensure a comprehensive assessment. Therefore, the performances of our proposed learners were evaluated in terms of four widely used statistical metrics, coefficient of determination (R^2), Nash-Sutcliffe efficiency (*NSE*), root mean square error (*RMSE*), and mean absolute error (*MAE*) [45, 85].

$$R^2 = \frac{\left[\sum_{i=1}^{n}\left(ET_{0p_i}-\overline{ET_{0p}}\right)\cdot\left(ET_{0PM_i}-\overline{ET_{0PM}}\right)\right]^2}{\sum_{i=1}^{n}\left(ET_{0p_i}-\overline{ET_{0p}}\right)\cdot\sum_{i=1}^{n}\left(ET_{0PM_i}-\overline{ET_{0PM}}\right)} \quad (3)$$

$$NSE = 1 - \frac{\sum_{i=1}^{n}\left(ET_{0PM_i}-ET_{0P_i}\right)^2}{\sum_{i=1}^{n}\left(ET_{0PM_i}-\overline{ET_{0PM}}\right)^2} \quad (4)$$

$$RMSE = \sqrt{\frac{\sum_{i=1}^{n}\left(ET_{0p_i}-ET_{0PM_i}\right)^2}{n}} \quad (5)$$

$$MAE = \frac{\sum_{i=1}^{n}\left|ET_{0p_i}-ET_{0PM_i}\right|}{n} \quad (6)$$

Where $ET_{0_{PM}}$ represents the FAO-56PM reference value of ET_0 (from equation 2), $ET_{0_{Pi}}$ refers to the estimated value of ET_0, $\overline{ET_{0PM}}$ is the mean of the reference value, $\overline{ET_{0P}}$ is the mean of the estimated value of ET_0, and n is the total number of input observations.

For comprehensive performance assessment and for better interpretation of the results, two composite metrics were formulated: average goodness (G_d) and average error (E_r). The G_d metric represents the arithmetic mean of two goodness-of-fit measures, the coefficient of determination (R^2) and Nash-Sutcliffe efficiency (*NSE*), mathematically expressed as

$$Gd = (R2 + NSE)/2 \quad (7)$$

Similarly, E_r represents the arithmetic mean of two error metrics: root mean square error (*RMSE*) and mean absolute error (*MAE*), expressed mathematically as

$$Er = (RMSE + MAE)/2 \quad (8)$$

A higher value of G_d represents a better fit, whereas a lower value of E_r indicates better performance of the model.

3. Results and Discussion

All the ensemble learners, along with their SI-optimized versions, were designed and applied in three study locations, Jalpaiguri, Cooch Behar, and Malda, in the North Bengal region.

Table 4. The values of performance metrics obtained against each model under eight input combinations at the study location, Jalpaiguri

	Combination C_1						**Combination C_2**						**Combination C_3**						**Combination C_4**					
	R^2	*NSE*	G_d	*RMSE*	*MAE*	E_r	R^2	*NSE*	G_d	*RMSE*	*MAE*	E_r	R^2	*NSE*	G_d	*RMSE*	*MAE*	E_r	R^2	*NSE*	G_d	*RMSE*	*MAE*	E_r
GBM	0.361	0.361	0.361	0.864	0.703	0.784	0.483	0.483	0.483	0.778	0.620	0.699	0.389	0.389	0.389	0.845	0.668	0.757	0.908	0.908	0.908	0.328	0.240	0.284
GBM+GWO	0.358	0.358	0.358	0.867	0.705	0.786	0.393	0.393	0.393	0.843	0.663	0.753	0.381	0.381	0.381	0.851	0.674	0.762	0.901	0.901	0.901	0.340	0.251	0.296
GBM+SFO	0.371	0.371	0.371	0.858	0.708	0.783	0.494	0.494	0.494	0.769	0.613	0.691	0.361	0.361	0.361	0.864	0.677	0.771	0.907	0.907	0.907	0.330	0.244	0.287
GBM+SSO	0.362	0.362	0.362	0.864	0.707	0.785	0.495	0.481	0.488	0.768	0.611	0.690	0.341	0.341	0.341	0.878	0.684	0.781	0.902	0.902	0.902	0.339	0.246	0.292
GBM+WOA	0.348	0.348	0.348	0.873	0.715	0.794	**0.511**	**0.511**	**0.511**	**0.756**	**0.604**	**0.680**	0.432	0.432	0.432	0.815	0.660	0.737	0.896	0.896	0.896	0.349	0.260	0.304
LGB	0.310	0.310	0.310	0.898	0.714	0.806	0.417	0.417	0.417	0.825	0.636	0.731	0.318	0.318	0.318	0.893	0.693	0.793	0.909	0.909	0.909	0.326	0.240	0.283
LGB+GWO	0.353	0.353	0.353	0.870	0.712	0.791	0.393	0.480	0.436	0.843	0.663	0.753	0.411	0.411	0.411	0.830	0.666	0.748	0.909	0.909	0.909	0.327	0.240	0.283
LGB+SFO	0.350	0.350	0.350	0.872	0.709	0.791	0.474	0.474	0.474	0.785	0.632	0.708	0.386	0.386	0.386	0.848	0.671	0.759	0.905	0.905	0.905	0.333	0.245	0.289
LGB+SSO	0.343	0.343	0.343	0.876	0.718	0.797	0.488	0.488	0.488	0.774	0.627	0.700	0.386	0.386	0.386	0.847	0.675	0.761	0.907	0.907	0.907	0.330	0.243	0.286
LGB+WOA	0.345	0.345	0.345	0.875	0.718	0.797	0.489	0.489	0.489	0.773	0.621	0.697	0.409	0.409	0.409	0.832	0.668	0.750	0.906	0.906	0.906	0.331	0.245	0.288
XGB	0.260	0.260	0.260	0.930	0.732	0.831	0.367	0.367	0.367	0.860	0.674	0.767	0.263	0.263	0.263	0.928	0.712	0.820	0.894	0.894	0.894	0.352	0.256	0.304
XGB+GWO	0.370	0.370	0.370	0.859	0.705	0.782	0.474	0.474	0.474	0.784	0.633	0.709	0.516	0.516	0.516	0.752	0.588	0.670	**0.910**	**0.910**	**0.910**	**0.325**	**0.238**	**0.281**
XGB+SFO	0.329	0.329	0.329	0.886	0.705	0.795	0.444	0.444	0.444	0.806	0.620	0.713	0.358	0.358	0.358	0.867	0.684	0.775	0.906	0.906	0.906	0.332	0.243	0.287
XGB+SSO	0.330	0.330	0.330	0.885	0.718	0.802	0.329	0.329	0.329	0.886	0.685	0.785	0.325	0.325	0.325	0.889	0.688	0.788	0.909	0.909	0.909	0.326	0.239	0.282
XGB+WOA	**0.418**	**0.418**	**0.418**	**0.825**	**0.677**	**0.751**	0.480	0.480	0.480	0.780	0.626	0.703	**0.528**	**0.528**	**0.528**	**0.743**	**0.574**	**0.659**	0.902	0.902	0.902	0.338	0.253	0.296
CAT	0.341	0.341	0.341	0.878	0.701	0.789	0.447	0.447	0.447	0.804	0.627	0.716	0.330	0.330	0.330	0.885	0.687	0.786	0.903	0.903	0.903	0.336	0.245	0.290
CAT+GWO	0.367	0.367	0.367	0.860	0.709	0.785	0.471	0.471	0.471	0.786	0.618	0.702	0.347	0.347	0.347	0.874	0.694	0.784	0.908	0.908	0.908	0.329	0.242	0.285
CAT+SFO	0.364	0.364	0.364	0.862	0.704	0.783	0.495	0.495	0.495	0.768	0.611	0.690	0.378	0.378	0.378	0.853	0.678	0.765	0.908	0.908	0.908	0.328	0.241	0.284
CAT+SSO	0.354	0.354	0.354	0.869	0.724	0.796	0.471	0.471	0.471	0.786	0.620	0.703	0.340	0.340	0.340	0.878	0.687	0.783	0.908	0.908	0.908	0.328	0.241	0.284
CAT+WOA	0.369	0.369	0.369	0.859	0.705	0.782	0.452	0.452	0.452	0.800	0.626	0.713	0.385	0.385	0.385	0.848	0.672	0.760	0.905	0.905	0.905	0.333	0.248	0.291

	Combination C_5						**Combination C_6**						**Combination C_7**						**Combination C_8**					
	R^2	*NSE*	G_d	*RMSE*	*MAE*	E_r	R^2	*NSE*	G_d	*RMSE*	*MAE*	E_r	R^2	*NSE*	G_d	*RMSE*	*MAE*	E_r	R^2	*NSE*	G_d	*RMSE*	*MAE*	E_r
GBM	0.541	0.541	0.541	0.732	0.585	0.659	0.962	0.962	0.962	0.210	0.159	0.184	0.889	0.889	0.889	0.361	0.264	0.313	0.962	0.962	0.962	0.212	0.158	0.185
GBM+GWO	0.500	0.500	0.500	0.765	0.611	0.688	0.967	0.967	0.967	0.197	0.151	0.174	0.874	0.874	0.874	0.384	0.277	0.330	0.972	0.972	0.972	0.182	0.134	0.158
GBM+SFO	0.499	0.499	0.499	0.765	0.598	0.682	**0.969**	**0.969**	**0.969**	**0.189**	**0.144**	**0.167**	0.888	0.888	0.888	0.362	0.273	0.318	0.969	0.969	0.969	0.191	0.139	0.165
GBM+SSO	0.535	0.535	0.535	0.737	0.587	0.662	0.963	0.963	0.963	0.207	0.153	0.180	0.864	0.864	0.864	0.398	0.286	0.342	0.971	0.971	0.971	0.184	0.135	0.160
GBM+WOA	0.512	0.512	0.512	0.755	0.587	0.671	0.968	0.968	0.968	0.193	0.144	0.169	0.891	0.891	0.891	0.357	0.273	0.315	**0.974**	**0.974**	**0.974**	**0.175**	**0.129**	**0.152**
LGB	0.478	0.478	0.478	0.781	0.609	0.695	0.956	0.956	0.956	0.227	0.163	0.195	0.870	0.870	0.870	0.390	0.278	0.334	0.959	0.959	0.959	0.219	0.153	0.186
LGB+GWO	0.553	0.553	0.553	0.723	0.577	0.650	0.960	0.960	0.960	0.216	0.155	0.185	0.890	0.890	0.890	0.359	0.264	0.312	0.966	0.966	0.966	0.200	0.142	0.171
LGB+SFO	0.534	0.534	0.534	0.738	0.590	0.664	0.961	0.961	0.961	0.212	0.156	0.184	0.879	0.879	0.879	0.376	0.273	0.324	0.963	0.963	0.963	0.209	0.150	0.179
LGB+SSO	0.525	0.525	0.525	0.745	0.587	0.666	0.960	0.960	0.960	0.216	0.153	0.184	0.890	0.890	0.890	0.359	0.267	0.313	0.968	0.968	0.968	0.194	0.140	0.167
LGB+WOA	0.539	0.539	0.539	0.734	0.592	0.663	0.960	0.960	0.960	0.215	0.156	0.186	0.891	0.891	0.891	0.357	0.260	0.308	0.965	0.965	0.965	0.201	0.144	0.173
XGB	0.480	0.480	0.480	0.780	0.606	0.693	0.960	0.960	0.960	0.216	0.158	0.187	0.858	0.858	0.858	0.407	0.291	0.349	0.955	0.955	0.955	0.230	0.162	0.196
XGB+GWO	0.519	0.519	0.519	0.750	0.600	0.675	0.966	0.966	0.966	0.198	0.147	0.172	**0.901**	**0.901**	**0.901**	**0.341**	**0.243**	**0.292**	0.962	0.962	0.962	0.212	0.153	0.182
XGB+SFO	0.511	0.511	0.511	0.756	0.598	0.677	0.965	0.965	0.965	0.203	0.149	0.176	0.879	0.879	0.879	0.377	0.277	0.327	0.960	0.960	0.960	0.216	0.154	0.185
XGB+SSO	0.452	0.452	0.452	0.800	0.616	0.708	0.965	0.965	0.965	0.201	0.146	0.174	0.859	0.859	0.859	0.406	0.290	0.348	0.962	0.962	0.962	0.210	0.145	0.178
XGB+WOA	**0.608**	**0.608**	**0.608**	**0.677**	**0.524**	**0.600**	0.967	0.967	0.967	0.196	0.145	0.170	0.899	0.899	0.899	0.344	0.245	0.295	0.968	0.968	0.968	0.192	0.136	0.164
CAT	0.512	0.512	0.512	0.756	0.598	0.677	0.965	0.965	0.965	0.203	0.149	0.176	0.868	0.868	0.868	0.393	0.281	0.337	0.964	0.964	0.964	0.204	0.141	0.172
CAT+GWO	0.523	0.523	0.523	0.747	0.593	0.670	0.968	0.968	0.968	0.195	0.147	0.171	0.869	0.869	0.869	0.391	0.282	0.337	0.961	0.961	0.961	0.214	0.151	0.183
CAT+SFO	0.490	0.490	0.490	0.772	0.610	0.691	0.967	0.967	0.967	0.196	0.151	0.173	0.877	0.877	0.877	0.379	0.278	0.329	0.961	0.961	0.961	0.212	0.152	0.182
CAT+SSO	0.498	0.498	0.498	0.766	0.614	0.690	0.965	0.965	0.965	0.202	0.152	0.177	0.852	0.852	0.852	0.416	0.292	0.354	0.963	0.963	0.963	0.209	0.152	0.181
CAT+WOA	0.568	0.568	0.568	0.711	0.573	0.642	0.965	0.965	0.965	0.201	0.154	0.178	0.889	0.889	0.889	0.360	0.266	0.313	0.949	0.949	0.949	0.244	0.175	0.210

Table 5. The values of performance metrics obtained against each model under eight input combinations atthe study location Cooch Behar

	Combination C_1						**Combination C_2**						**Combination C_3**						**Combination C_4**					
	R^2	*NSE*	G_d	*RMSE*	*MAE*	E_r	R^2	*NSE*	G_d	*RMSE*	*MAE*	E_r	R^2	*NSE*	G_d	*RMSE*	*MAE*	E_r	R^2	*NSE*	G_d	*RMSE*	*MAE*	E_r
GBM	0.314	0.314	0.314	1.013	0.746	0.879	0.415	0.415	0.415	0.935	0.696	0.816	0.722	0.722	0.722	0.645	0.471	0.558	0.874	0.874	0.874	0.434	0.257	0.346
GBM+GWO	0.321	0.321	0.321	1.007	0.750	0.878	**0.431**	**0.431**	**0.431**	**0.922**	**0.685**	**0.804**	0.689	0.689	0.689	0.682	0.494	0.588	0.869	0.869	0.869	0.442	0.261	0.352
GBM+SFO	0.350	0.350	0.350	0.986	0.734	0.860	0.414	0.414	0.414	0.936	0.694	0.815	0.701	0.701	0.701	0.669	0.480	0.575	0.871	0.871	0.871	0.439	0.260	0.350
GBM+SSO	0.341	0.341	0.341	0.992	0.737	0.865	0.399	0.399	0.399	0.948	0.704	0.826	0.724	0.724	0.724	0.642	0.468	0.555	0.876	0.876	0.876	0.430	0.255	0.343
GBM+WOA	0.334	0.334	0.334	0.997	0.728	0.863	0.402	0.402	0.402	0.945	0.704	0.825	0.722	0.722	0.722	0.644	0.469	0.557	0.872	0.872	0.872	0.438	0.263	0.351
LGB	0.290	0.290	0.290	1.030	0.761	0.895	0.343	0.343	0.343	0.991	0.727	0.859	0.718	0.718	0.718	0.650	0.468	0.559	0.874	0.874	0.874	0.433	0.256	0.345
LGB+GWO	0.346	0.346	0.346	0.989	0.736	0.863	0.397	0.397	0.397	0.950	0.704	0.827	0.716	0.716	0.716	0.651	0.473	0.562	0.871	0.871	0.871	0.439	0.260	0.349
LGB+SFO	0.328	0.328	0.328	1.002	0.745	0.873	0.425	0.425	0.425	0.927	0.689	0.808	**0.747**	**0.747**	**0.747**	**0.614**	**0.451**	**0.533**	0.866	0.866	0.866	0.447	0.266	0.356
LGB+SSO	0.343	0.343	0.343	0.991	0.734	0.863	0.428	0.428	0.428	0.925	0.686	0.805	0.712	0.712	0.712	0.656	0.476	0.566	0.875	0.875	0.875	0.433	0.259	0.346
LGB+WOA	0.336	0.336	0.336	0.996	0.729	0.862	0.393	0.393	0.393	0.952	0.707	0.830	0.726	0.726	0.726	0.640	0.460	0.550	0.862	0.862	0.862	0.454	0.275	0.364
XGB	0.179	0.179	0.179	1.108	0.808	0.958	0.261	0.261	0.261	1.051	0.768	0.910	0.681	0.681	0.681	0.691	0.501	0.596	0.864	0.864	0.864	0.451	0.274	0.362
XGB+GWO	0.338	0.338	0.338	0.995	0.736	0.865	0.407	0.407	0.407	0.941	0.698	0.820	0.736	0.736	0.736	0.628	0.461	0.545	0.874	0.874	0.874	0.433	0.258	0.346
XGB+SFO	0.320	0.320	0.320	1.008	0.745	0.877	0.383	0.383	0.383	0.960	0.705	0.833	0.716	0.716	0.716	0.651	0.477	0.564	0.876	0.876	0.876	0.431	0.253	0.342
XGB+SSO	0.236	0.236	0.236	1.069	0.790	0.929	0.379	0.379	0.379	0.963	0.712	0.838	0.663	0.663	0.663	0.710	0.504	0.607	0.872	0.872	0.872	0.438	0.256	0.347
XGB+WOA	0.323	0.323	0.323	1.006	0.745	0.875	0.405	0.405	0.405	0.943	0.693	0.818	0.722	0.722	0.722	0.645	0.472	0.558	0.869	0.869	0.869	0.442	0.264	0.353
CAT	0.262	0.262	0.262	1.050	0.776	0.913	0.329	0.329	0.329	1.002	0.732	0.867	0.706	0.706	0.706	0.663	0.479	0.571	0.873	0.873	0.873	0.435	0.261	0.348
CAT+GWO	0.328	0.328	0.328	1.002	0.753	0.877	0.428	0.428	0.428	0.925	0.687	0.806	0.720	0.720	0.720	0.647	0.470	0.559	0.876	0.876	0.876	0.431	0.253	0.342
CAT+SFO	0.348	0.348	0.348	0.987	0.732	0.859	0.426	0.426	0.426	0.926	0.688	0.807	0.741	0.741	0.741	0.622	0.452	0.537	**0.878**	**0.878**	**0.878**	**0.426**	**0.247**	**0.337**
CAT+SSO	**0.354**	**0.354**	**0.354**	**0.982**	**0.730**	**0.856**	0.427	0.427	0.427	0.926	0.690	0.808	0.738	0.738	0.738	0.626	0.459	0.543	0.874	0.874	0.874	0.433	0.256	0.344
CAT+WOA	0.346	0.346	0.346	0.989	0.746	0.868	0.392	0.392	0.392	0.954	0.709	0.831	0.717	0.717	0.717	0.651	0.478	0.564	0.877	0.877	0.877	0.428	0.250	0.339

	Combination C_5						Combination C_6						Combination C_7						Combination C_8					
	R^2	NSE	G_d	RMSE	MAE	E_r	R^2	NSE	G_d	RMSE	MAE	E_r	R^2	NSE	G_d	RMSE	MAE	E_r	R^2	NSE	G_d	RMSE	MAE	E_r
GBM	0.828	0.828	0.828	0.507	0.383	0.445	0.919	0.919	0.919	0.348	0.189	0.269	0.878	0.878	0.878	0.427	0.245	0.336	0.928	0.928	0.928	0.328	0.159	0.243
GBM+GWO	0.821	0.821	0.821	0.517	0.385	0.451	0.923	0.923	0.923	0.339	0.178	0.258	0.879	0.879	0.879	0.426	0.246	0.336	0.953	0.953	0.953	0.265	0.130	0.198
GBM+SFO	0.810	0.810	0.810	0.533	0.398	0.466	**0.937**	**0.937**	**0.937**	**0.307**	**0.174**	**0.240**	0.879	0.879	0.879	0.425	0.240	0.332	0.953	0.953	0.953	0.266	0.136	0.201
GBM+SSO	0.818	0.818	0.818	0.521	0.390	0.455	0.914	0.914	0.914	0.358	0.191	0.275	0.877	0.877	0.877	0.429	0.250	0.339	0.950	0.950	0.950	0.275	0.133	0.204
GBM+WOA	0.822	0.822	0.822	0.515	0.389	0.452	0.934	0.934	0.934	0.314	0.181	0.247	0.881	0.881	0.881	0.422	0.242	0.332	0.958	0.958	0.958	0.251	0.129	0.190
LGB	0.794	0.794	0.794	0.555	0.406	0.480	0.910	0.910	0.910	0.367	0.191	0.279	0.882	0.882	0.882	0.420	0.238	0.329	0.925	0.925	0.925	0.335	0.153	0.244
LGB+GWO	0.821	0.821	0.821	0.517	0.379	0.448	0.926	0.926	0.926	0.332	0.176	0.254	0.883	0.883	0.883	0.419	0.246	0.332	0.944	0.944	0.944	0.289	0.140	0.215
LGB+SFO	0.828	0.828	0.828	0.507	0.377	0.442	0.925	0.925	0.925	0.335	0.179	0.257	0.882	0.882	0.882	0.420	0.243	0.332	0.941	0.941	0.941	0.297	0.136	0.217
LGB+SSO	0.822	0.822	0.822	0.515	0.386	0.451	0.920	0.920	0.920	0.346	0.179	0.263	0.881	0.881	0.881	0.423	0.246	0.334	0.941	0.941	0.941	0.298	0.143	0.220
LGB+WOA	0.815	0.815	0.815	0.525	0.389	0.457	0.924	0.924	0.924	0.336	0.178	0.257	0.882	0.882	0.882	0.420	0.241	0.330	0.938	0.938	0.938	0.305	0.141	0.223
XGB	0.767	0.767	0.767	0.591	0.435	0.513	0.912	0.912	0.912	0.362	0.191	0.276	0.876	0.876	0.876	0.430	0.247	0.339	0.927	0.927	0.927	0.331	0.158	0.244
XGB+GWO	**0.826**	**0.826**	**0.826**	**0.510**	**0.384**	**0.447**	0.920	0.920	0.920	0.345	0.185	0.265	0.882	0.882	0.882	0.420	0.237	0.329	0.955	0.955	0.955	0.258	0.129	0.193
XGB+SFO	0.823	0.823	0.823	0.515	0.380	0.447	0.922	0.922	0.922	0.341	0.180	0.260	0.876	0.876	0.876	0.431	0.254	0.342	0.936	0.936	0.936	0.309	0.147	0.228
XGB+SSO	0.785	0.785	0.785	0.567	0.421	0.494	0.912	0.912	0.912	0.363	0.190	0.276	0.880	0.880	0.880	0.423	0.241	0.332	0.953	0.953	0.953	0.264	0.134	0.199
XGB+WOA	0.807	0.807	0.807	0.537	0.393	0.465	0.928	0.928	0.928	0.329	0.179	0.254	0.880	0.880	0.880	0.423	0.243	0.333	0.955	0.955	0.955	0.259	0.138	0.198
CAT	0.814	0.814	0.814	0.527	0.396	0.462	0.931	0.931	0.931	0.321	0.179	0.250	0.882	0.882	0.882	0.419	0.239	0.329	0.943	0.943	0.943	0.292	0.132	0.212
CAT+GWO	0.840	0.840	0.840	0.489	0.367	0.428	0.921	0.921	0.921	0.344	0.176	0.260	**0.886**	**0.886**	**0.886**	**0.412**	**0.237**	**0.325**	0.946	0.946	0.946	0.284	0.132	0.208
CAT+SFO	0.833	0.833	0.833	0.499	0.381	0.440	0.928	0.928	0.928	0.329	0.175	0.252	0.882	0.882	0.882	0.421	0.246	0.333	**0.960**	**0.960**	**0.960**	**0.245**	**0.133**	**0.189**
CAT+SSO	0.835	0.835	0.835	0.497	0.383	0.440	0.924	0.924	0.924	0.337	0.178	0.257	0.882	0.882	0.882	0.420	0.245	0.333	0.943	0.943	0.943	0.291	0.136	0.213
CAT+WOA	0.843	0.843	0.843	0.485	0.367	0.426	0.936	0.936	0.936	0.308	0.172	0.240	0.886	0.886	0.886	0.413	0.234	0.323	0.954	0.954	0.954	0.262	0.139	0.200

Table 6. The values of performance metrics obtained against each model under eight input combinationsthe at study location Malda

	Combination C_1						**Combination C_2**						**Combination C_3**						**Combination C_4**					
	R^2	*NSE*	G_d	*RMSE*	*MAE*	E_r	R^2	*NSE*	G_d	*RMSE*	*MAE*	E_r	R^2	*NSE*	G_d	*RMSE*	*MAE*	E_r	R^2	*NSE*	G_d	*RMSE*	*MAE*	E_r
GBM	0.597	0.597	0.597	0.697	0.565	0.631	0.610	0.611	0.610	0.686	0.551	0.618	0.753	0.753	0.753	0.546	0.419	0.482	0.966	0.966	0.966	0.201	0.153	0.177
GBM+GWO	0.578	0.578	0.578	0.714	0.579	0.647	0.603	0.603	0.603	0.692	0.552	0.622	0.751	0.751	0.751	0.548	0.421	0.485	0.969	0.969	0.969	0.195	0.146	0.170
GBM+SFO	0.579	0.579	0.579	0.712	0.582	0.647	0.614	0.614	0.614	0.682	0.549	0.616	0.759	0.759	0.759	0.539	0.416	0.477	0.966	0.966	0.966	0.202	0.152	0.177
GBM+SSO	0.477	0.477	0.477	0.795	0.638	0.717	0.610	0.610	0.610	0.686	0.549	0.618	0.759	0.759	0.759	0.539	0.411	0.475	0.966	0.966	0.966	0.202	0.153	0.178
GBM+WOA	0.564	0.564	0.564	0.725	0.589	0.657	0.594	0.594	0.594	0.700	0.559	0.629	0.745	0.745	0.745	0.555	0.429	0.492	0.964	0.964	0.964	0.209	0.154	0.182
LGB	0.595	0.595	0.595	0.699	0.559	0.629	0.585	0.585	0.585	0.707	0.560	0.634	0.722	0.722	0.722	0.579	0.441	0.510	0.961	0.961	0.961	0.218	0.167	0.192
LGB+GWO	0.595	0.595	0.595	0.699	0.566	0.633	0.622	0.622	0.622	0.676	0.540	0.608	0.757	0.757	0.757	0.541	0.419	0.480	0.967	0.967	0.967	0.199	0.152	0.176
LGB+SFO	0.607	0.607	0.607	0.688	0.554	0.621	0.545	0.545	0.545	0.741	0.601	0.671	0.757	0.757	0.757	0.541	0.419	0.480	0.964	0.964	0.964	0.207	0.160	0.184
LGB+SSO	0.605	0.605	0.605	0.690	0.556	0.623	**0.625**	**0.625**	**0.625**	**0.673**	**0.541**	**0.607**	0.721	0.721	0.721	0.580	0.449	0.514	0.966	0.966	0.966	0.202	0.153	0.177
LGB+WOA	0.573	0.573	0.573	0.718	0.583	0.651	0.603	0.603	0.603	0.692	0.558	0.625	0.755	0.755	0.755	0.543	0.419	0.481	0.962	0.962	0.962	0.213	0.162	0.187
XGB	0.542	0.542	0.542	0.743	0.598	0.671	0.505	0.505	0.505	0.773	0.613	0.693	0.653	0.653	0.653	0.647	0.494	0.570	0.959	0.959	0.959	0.223	0.172	0.198
XGB+GWO	**0.608**	**0.608**	**0.608**	**0.688**	**0.549**	**0.619**	0.591	0.591	0.591	0.703	0.566	0.635	0.759	0.759	0.759	0.539	0.414	0.477	0.966	0.966	0.966	0.201	0.154	0.178
XGB+SFO	0.598	0.598	0.598	0.696	0.558	0.627	0.615	0.615	0.615	0.682	0.546	0.614	0.696	0.696	0.696	0.605	0.465	0.535	0.967	0.967	0.967	0.200	0.152	0.176
XGB+SSO	0.605	0.605	0.605	0.690	0.557	0.624	0.600	0.600	0.600	0.694	0.553	0.624	0.717	0.717	0.717	0.584	0.448	0.516	0.963	0.963	0.963	0.211	0.159	0.185
XGB+WOA	0.603	0.603	0.603	0.692	0.542	0.617	0.607	0.607	0.607	0.689	0.537	0.613	**0.768**	**0.768**	**0.768**	**0.529**	**0.407**	**0.468**	0.960	0.960	0.960	0.219	0.169	0.194
CAT	0.566	0.566	0.566	0.724	0.582	0.653	0.565	0.565	0.565	0.725	0.574	0.649	0.712	0.712	0.712	0.589	0.454	0.522	0.965	0.965	0.965	0.206	0.156	0.181
CAT+GWO	0.603	0.603	0.603	0.692	0.560	0.626	0.609	0.609	0.609	0.687	0.548	0.617	0.764	0.764	0.764	0.534	0.414	0.474	0.965	0.965	0.965	0.205	0.154	0.180
CAT+SFO	0.598	0.598	0.598	0.696	0.563	0.630	0.621	0.621	0.621	0.676	0.540	0.608	0.760	0.760	0.760	0.538	0.412	0.475	0.969	0.969	0.969	0.194	0.150	0.172
CAT+SSO	0.605	0.605	0.605	0.691	0.561	0.626	**0.624**	**0.624**	**0.624**	**0.673**	**0.537**	**0.605**	0.759	0.759	0.759	0.539	0.415	0.477	**0.970**	**0.970**	**0.970**	**0.192**	**0.149**	**0.170**
CAT+WOA	0.605	0.605	0.605	0.690	0.555	0.623	0.602	0.602	0.602	0.693	0.554	0.623	0.760	0.760	0.760	0.538	0.412	0.475	0.967	0.967	0.967	0.200	0.152	0.176

	Combination C_5						Combination C_6						Combination C_7						Combination C_8					
	R^2	NSE	G_d	RMSE	MAE	E_r	R^2	NSE	G_d	RMSE	MAE	E_r	R^2	NSE	G_d	RMSE	MAE	E_r	R^2	NSE	G_d	RMSE	MAE	E_r
GBM	0.762	0.762	0.762	0.536	0.420	0.478	0.958	0.958	0.958	0.224	0.176	0.200	0.969	0.969	0.969	0.195	0.145	0.170	0.963	0.963	0.963	0.212	0.168	0.190
GBM+GWO	0.746	0.746	0.746	0.554	0.441	0.498	0.956	0.956	0.956	0.230	0.183	0.206	0.969	0.969	0.969	0.194	0.147	0.171	0.964	0.964	0.964	0.208	0.164	0.186
GBM+SFO	0.672	0.672	0.672	0.629	0.508	0.569	0.957	0.957	0.957	0.227	0.179	0.203	0.963	0.963	0.963	0.211	0.152	0.181	0.967	0.967	0.967	0.200	0.157	0.179
GBM+SSO	0.726	0.726	0.726	0.575	0.449	0.512	0.955	0.955	0.955	0.234	0.186	0.210	0.965	0.965	0.965	0.204	0.153	0.179	0.967	0.967	0.967	0.201	0.158	0.179
GBM+WOA	0.750	0.750	0.750	0.549	0.434	0.492	0.959	0.959	0.959	0.222	0.176	0.199	0.970	0.970	0.970	0.189	0.139	0.164	0.964	0.964	0.964	0.208	0.165	0.187
LGB	0.742	0.742	0.742	0.558	0.438	0.498	0.955	0.955	0.955	0.233	0.181	0.207	0.962	0.962	0.962	0.215	0.160	0.188	0.962	0.962	0.962	0.215	0.167	0.191
LGB+GWO	0.744	0.744	0.744	0.556	0.441	0.498	0.958	0.958	0.958	0.226	0.177	0.202	0.969	0.969	0.969	0.193	0.141	0.167	0.962	0.962	0.962	0.214	0.167	0.191
LGB+SFO	0.755	0.755	0.755	0.544	0.430	0.487	0.957	0.957	0.957	0.228	0.177	0.202	0.970	0.970	0.970	0.190	0.140	0.165	0.968	0.968	0.968	0.197	0.153	0.175
LGB+SSO	0.749	0.749	0.749	0.550	0.439	0.494	0.954	0.954	0.954	0.235	0.183	0.209	0.969	0.969	0.969	0.194	0.146	0.170	0.967	0.967	0.967	0.201	0.157	0.179
LGB+WOA	0.754	0.754	0.754	0.545	0.434	0.489	0.955	0.955	0.955	0.234	0.182	0.208	0.970	0.970	0.970	0.191	0.144	0.167	0.968	0.968	0.968	0.197	0.153	0.175
XGB	0.691	0.691	0.691	0.610	0.485	0.547	0.954	0.954	0.954	0.235	0.179	0.207	0.954	0.954	0.954	0.237	0.180	0.208	0.958	0.958	0.958	0.224	0.169	0.196
XGB+GWO	0.747	0.747	0.747	0.552	0.438	0.495	0.958	0.958	0.958	0.225	0.180	0.202	0.967	0.967	0.967	0.200	0.146	0.173	0.968	0.968	0.968	0.198	0.154	0.176
XGB+SFO	0.758	0.758	0.758	0.540	0.430	0.485	0.957	0.957	0.957	0.227	0.179	0.203	0.962	0.962	0.962	0.214	0.159	0.187	0.963	0.963	0.963	0.212	0.165	0.189
XGB+SSO	0.746	0.746	0.746	0.553	0.438	0.495	0.953	0.953	0.953	0.238	0.186	0.212	0.967	0.967	0.967	0.201	0.150	0.175	0.959	0.959	0.959	0.223	0.169	0.196
XGB+WOA	0.740	0.740	0.740	0.560	0.438	0.499	0.960	0.960	0.960	0.221	0.174	0.197	0.971	0.971	0.971	0.188	0.141	0.165	0.965	0.965	0.965	0.206	0.162	0.184
CAT	0.727	0.727	0.727	0.574	0.459	0.517	0.957	0.957	0.957	0.228	0.179	0.203	0.966	0.966	0.966	0.202	0.152	0.177	0.965	0.965	0.965	0.204	0.160	0.182
CAT+GWO	0.755	0.755	0.755	0.544	0.426	0.485	0.958	0.958	0.958	0.226	0.179	0.203	0.971	0.971	0.971	0.186	0.137	0.162	**0.970**	**0.970**	**0.970**	**0.191**	**0.151**	**0.171**
CAT+SFO	0.756	0.756	0.756	0.543	0.428	0.486	0.953	0.953	0.953	0.239	0.193	0.216	0.972	0.972	0.972	0.183	0.138	0.160	0.966	0.966	0.966	0.201	0.159	0.180
CAT+SSO	0.745	0.745	0.745	0.555	0.435	0.495	**0.962**	**0.962**	**0.962**	**0.214**	**0.171**	**0.193**	0.973	0.973	0.973	0.180	0.135	0.158	0.968	0.968	0.968	0.197	0.155	0.176
CAT+WOA	**0.768**	**0.768**	**0.768**	**0.529**	**0.415**	**0.472**	0.956	0.956	0.956	0.231	0.183	0.207	**0.973**	**0.973**	**0.973**	**0.180**	**0.134**	**0.157**	0.966	0.966	0.966	0.202	0.168	0.185

The performance of each learner was evaluated in terms of goodness metric (G_d) and error metric (E_r), as defined in equations 7 and 8. The standard values ET_{0PM} obtained using the FAO-56PM method (equation 2) were considered as the reference values of ET_0. The empirical results are presented in Tables 4 to 6.

3.1 Impact of Coupling of Optimizers on the Performance of the Ensemble Learners

The impact of the coupling of the four SI optimizers on each of the four primary learners was studied at three locations. A comparative analysis was conducted between the average performance of the primary learners and their four optimized variants (learner-optimizer pairs) over eight input combinations (C_1 to C_8). To study the overall performance of each learner, the average values (G_{avg}) of goodness metric G_d and the average values (E_{avg}) of error metric E_r obtained against eight input combinations at each study location were considered as comparison criteria. These two average values are defined as:

$$G_{avg}=\frac{1}{8}\sum_{i=1}^{8} G_d \quad (9)$$

$$E_{avg}=\frac{1}{8}\sum_{i=1}^{8} E_r \quad (10)$$

For the study ,location Jalpaiguri, the GBM coupled with WOA optimizer (GBM+WOA) performed better (with G_{avg} = 0.692 and E_{avg} = 0.478) than the primary learner (with G_{avg} = 0.687 and E_{avg} = 0.483) as illustrated in Figure 3(a). The other optimized versions of GBM were comparatively less performing (with G_{avg} ranging from 0.668 to 0.682 and E_{avg} ranging from 0.483 to 0.493), respectively and all of the optimized versions of the LGB learner outperformed the primary learner, as shown in Figure 3(b). The LGB learner coupled with the WOA optimizer (LGB+WOA) revealed the best performance among the four optimized versions of the LGB learner. Figures. 3(c) and 3(d) illustrate that all the optimized versions of XGB and CAT performed better than their respective primary learner. When XGB was optimized with WOA (XGB+WOA), it produced the best result (with G_{avg} = 0.721 and E_{avg} = 0.455) among the other versions of XGB. A similar effect was observed in the case of CAT when optimized with WOA (CAT+WOA) (with G_{avg} = 0.685 and E_{avg} = 0.486).

Figures 4(a-d) depict that for the study location Cooch Behar, all the optimized versions of GBM outperformed their respective primary learners in terms of G_{avg} and E_{avg}. The GBM optimized with WOA (GBM+WOA) exhibited the best performance (with G_{avg} = 0.741 and E_{avg} = 0.477) compared to the other versions, as shown in Figure 4(a). The GBM+SFO learner also showed a nearly equal performance (with G_{avg} = 0.739 and E_{avg} = 0.480). Figure 4(b) depicts that the (LGB+SFO) learner performed best (with G_{avg} = 0.743 and E_{avg} = 0.477) among the other versions of LGB. When XGB was coupled with the GWO optimizer (XGB+GWO), the learner produced the best performance (with G_{avg} = 0.742 and E_{avg} = 0.476), as shown in Figure 4(c). Figure 4(d) illustrates that the CAT learner optimized with SFO outperformed the other versions in terms of G_{avg} and E_{avg} (with G_{avg} = 0.750 and E_{avg} = 0.469). This observation is very similar to that of the LGB.

For the study location Malda, as an exception, the GBM primary learner (with G_{avg} = 0.822 and E_{avg} = 0.360) outperformed its other optimized versions with (G_{avg} ranging from 0.803 to 0.817 and E_{avg} ranging from 0.365 to 0.374), as projected in Figure. 5(a). Figure 5(b) depicts that all the optimized versions of LGB dominated the primary learner LGB (with G_{avg} = 0.810 and E_{avg} = 0.372). The LGB coupled with GWO (LGB+GWO) was the best performer (G_{avg} = 0.822 and E_{avg} = 0.361). Figure 5(c) shows that the primary learner XGB coupled with whale optimizer (XGB+WOA) produced superior results (with G_{avg} = 0.822 and E_{avg} = 0.358) than the primary learner (with G_{avg} = 0.777 and E_{avg} = 0.402). Compared to the other optimized versions, the CAT performed worse in terms of G_{avg} (= 0.803) and E_{avg} (= 0.377). This observation similar identical to those obtained for the other two locations. Figure 5 (d) depicts that the CAT+SSO is the best learner for Malda (with G_{avg} = 0.826 and E_{avg} = 0.354).

3.2 Selection of the Best Learner-Optimizer Pair in the Data Limited Scenario

Table 4 depicts that at the study location, Jalpaiguri, the performances of all the learners were not remarkable enough against the input combination C_1, C_2, C_3, and C_5. The XGB+WOA learner was the most appropriate for the input combinations C_1, C_3, and C_5 (with G_d ranging from 0.418 to 0.608 and E_r ranging from 0.600 to 0.751). For input combinations C_2 and C_8, the GBM+WOA hybrid learner achieved optimal performance, yielding the highest accuracy scores with (G_d = 0.511, E_r = 0.680) and (G_d = 0.974, E_r = 0.152), respectively. The XGB+GWO model exhibited the best performance for the input combinations C_4 and C_7. The experimental results from C_4 and C_7 demonstrated G_d values within the interval of 0.901 to 0.910 and E_r values within the range of 0.281 to 0.292. It may be noted that the GBM+SFO hybrid model exhibited superior performance for input combination C_6, achieving optimal G_d = 0.969 and E_r = 0.167.

It is exposed from Table 5 that at the study location Cooch Behar, the performances of all the learners were not satisfactory against the input combination C_1. However, the CAT+SSO model was the best choice among all the learners, with G_d = 0.354 and E_r = 0.856. For input combination C_2, the GBM+GWO learner revealed relatively better performance with G_d = 0.431 and E_r = 0.804.

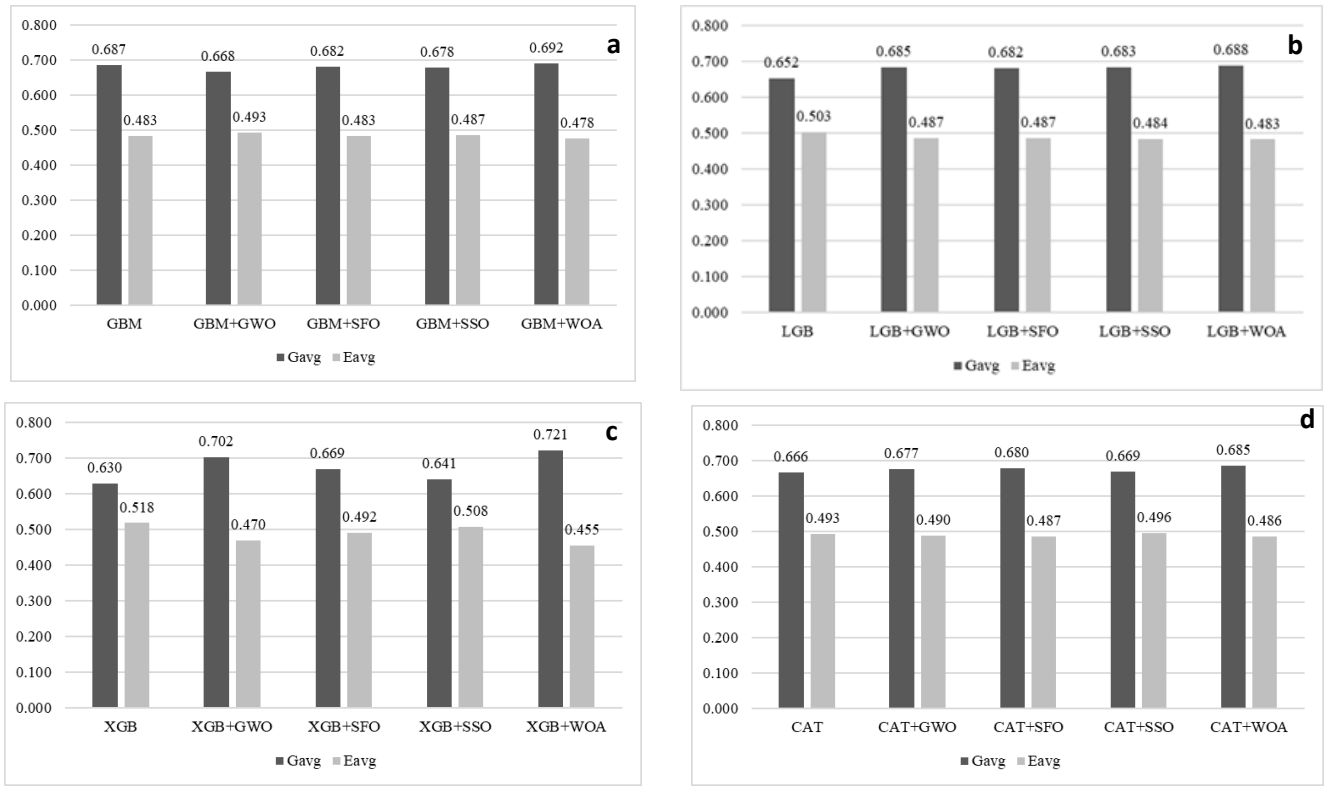

Figure 3. G_{avg} and E_{avg} values of (a) GBM, (b) LGB, (c) XGB, and (d) CAT primary learners, along with their optimized variants for Jalpaiguri. The bar charts indicate that all the primary learners exhibit relatively good performance. Though in some instances optimized learners perform better, in other cases they exhibit poorer results than the primary learners. It is clear from the bar charts that the effectiveness of optimized learners depends heavily on the specific optimizer used.

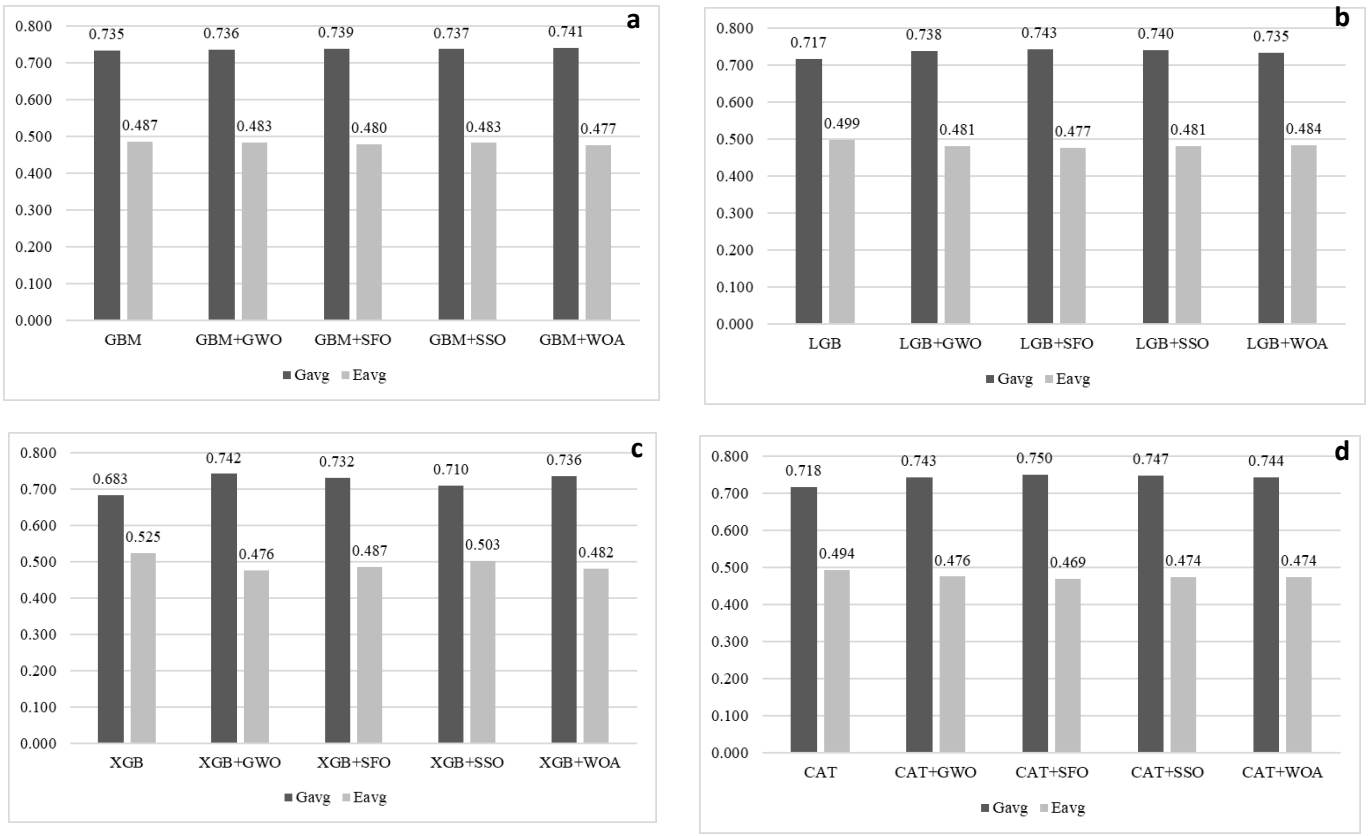

Figure 4. G_{avg} and E_{avg} values of (a) GBM, (b) LGB, (c) XGB, and (d) CAT primary learners, along with their optimized variants for Cooch Behar. The bar charts depict that all the primary learners exhibit relatively poor accuracy than the optimized learners

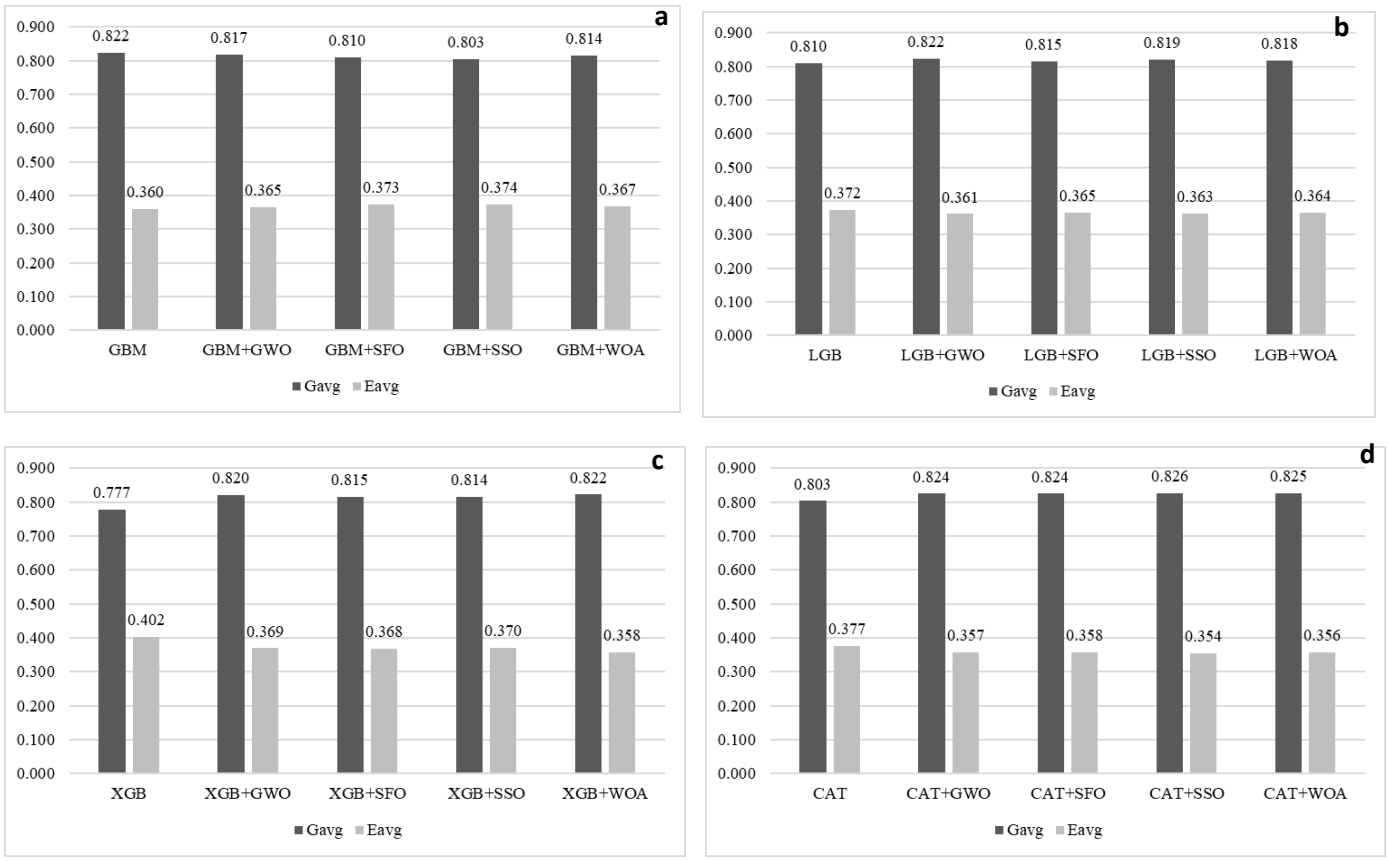

Figure 5. G_{avg} and E_{avg} values of (a) GBM, (b) LGB, (c) XGB, and (d) CAT primary learners, along with their optimized variants for Malda. The CAT+SSO model achieved the highest G_{avg} value (=0.826), while all the optimized versions of the GBM model underperform than the primary learner GBM, showing that optimization effectiveness varies from learner to learner.

The LGB+SFO learner was the most appropriate for the input combination C_3 with G_d = 0.747 and E_r = 0.533. The CAT+SFO learner exhibited the best performance against the combinations C_4 and C_8, both in terms of the highest values of G_d (ranging from 0.878 to 0.960 and hed lowest values of E_r (ranging from 0.337 to 0.189). For input combinations C_5, C_6, and C_7, the hybrid models XGB-GWO, GBM-SFO, and CAT-GWO demonstrated superior performance compared to alternative learners, achieving G_d values between 0.826 and 0.937 and E_r values ranging from 0.240 to 0.447.

The performances of all the learners were not appreciable against the input combination C_1 at Malda. Table 6 illustrates that the XGB+GWO learner was the best choice for input combination C_1 (G_d = 0.608 and E_r = 0.619). For input combination C_2, the performance of LGB+SSO was almost equal to that of the CAT+SSO learner with (G_d = 0.625 and E_r = 0.607) and (G_d = 0.624 and E_r = 0.605), respectively. From Table 6, it is observed that the XGB+WOA model exhibited the best performance for input combination C_3, having G_d = 0.768 and E_r = 0.468. For the input combinations C_4 and C_6, the CAT+SSO learner outperformed the other versions, with (G_d ranging from 0.962 to 0.970 and E_r ranging from 0.170 to 0.193). One of the optimized versions of the CAT learner (CAT+WOA), was the most appropriate learner for the input combinations C_5 and C_7, while the other version of CAT, CAT+GWO) learner, was the best performer for input combination C_8 w,ith (G_d = 0.970 and E_r = 0.171).

Table 7 presents the empirical performance metrics (G_d and E_r) for model selection across different input combinations at the three study locations. It is inferred from Table 7 that no single learner can be the best one for all the input combinations irrespective of the study locations; instead, the best learner should be chosen based on the location and available input combinations.

3.3 Impact of Different Input Combinations on Estimation Accuracy of ET_0

The values of ET_0 were estimated against different input combinations at three study locations in terms of the selected best-performing learner. For each input combination, the estimated values of ET_0 are scatter plotted against the standard reference values of ET_{0PM} obtained using the FAO-56PM method (equation 2). Figures 6 through 8 present scatter plots comparing the performance across eight input combinations (C_1 to C_8) for the three study locations: Jalpaiguri, Cooch Behar, and Malda, respectively. From the scatter plots presented in Figures 6(a), 7(a), and 8(a), it is evident that input combination C_1 consisting of only two parameters

T_{min} and T_{max} produced the worst results (with R^2 ranging from 0.354 to 0.608, *NSE* ranging from 0.354 to 0.608, *RMSE* ranging from 0.688 to 0.982 and, *MAE* ranging from 0.619 to 0.730) at three locations and should not be considered for ET_0 estimation.

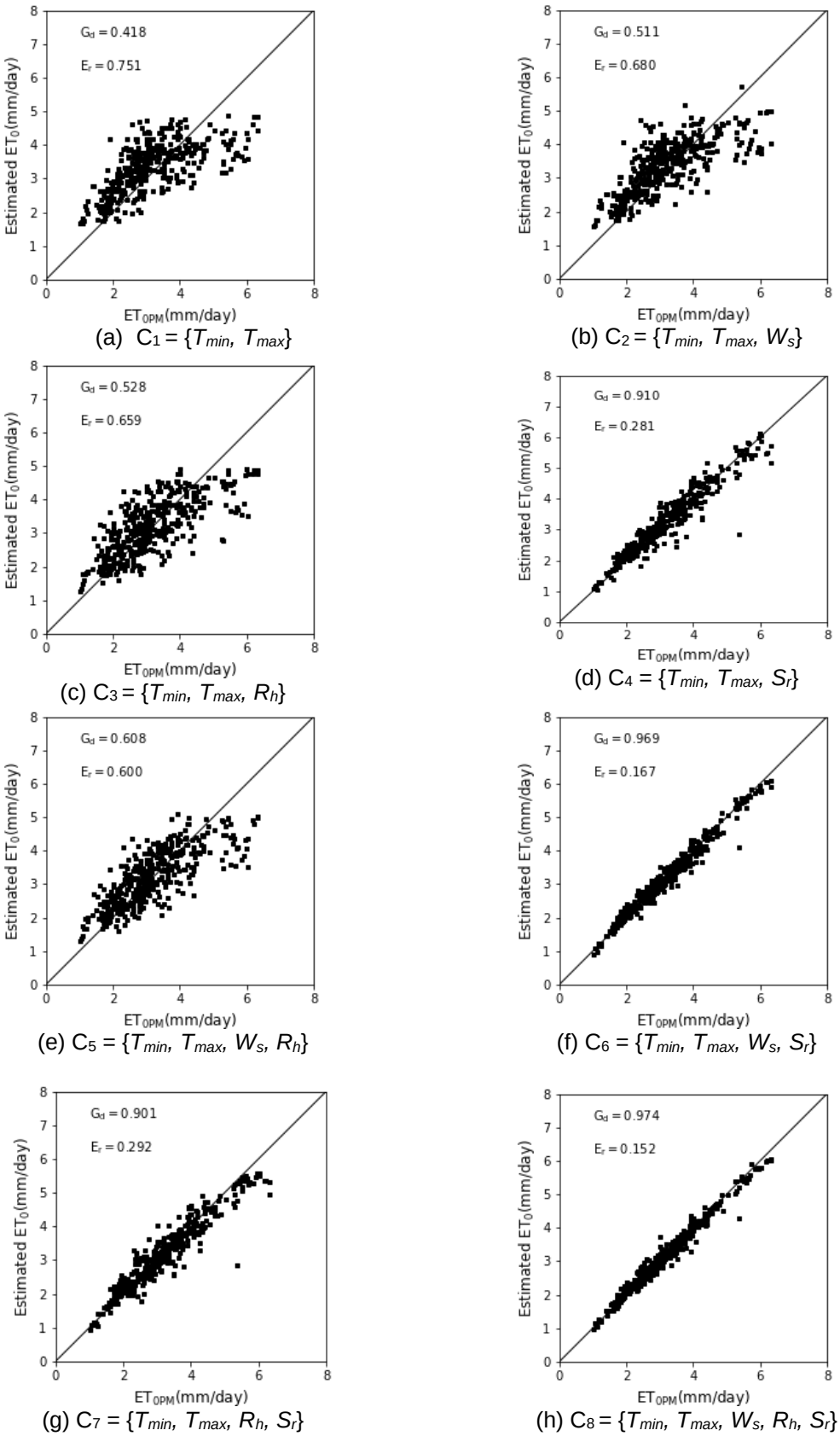

Figure 6. Scatter plots for eight combinations of inputs for Jalpaiguri. According to e scatter plots, the estimated ET_0 from the input combinations C_4, C_6, and C_8 is comparatively accurate, indicating these input combinations are suitable for estimating ET_0 at Jalpaiguri.

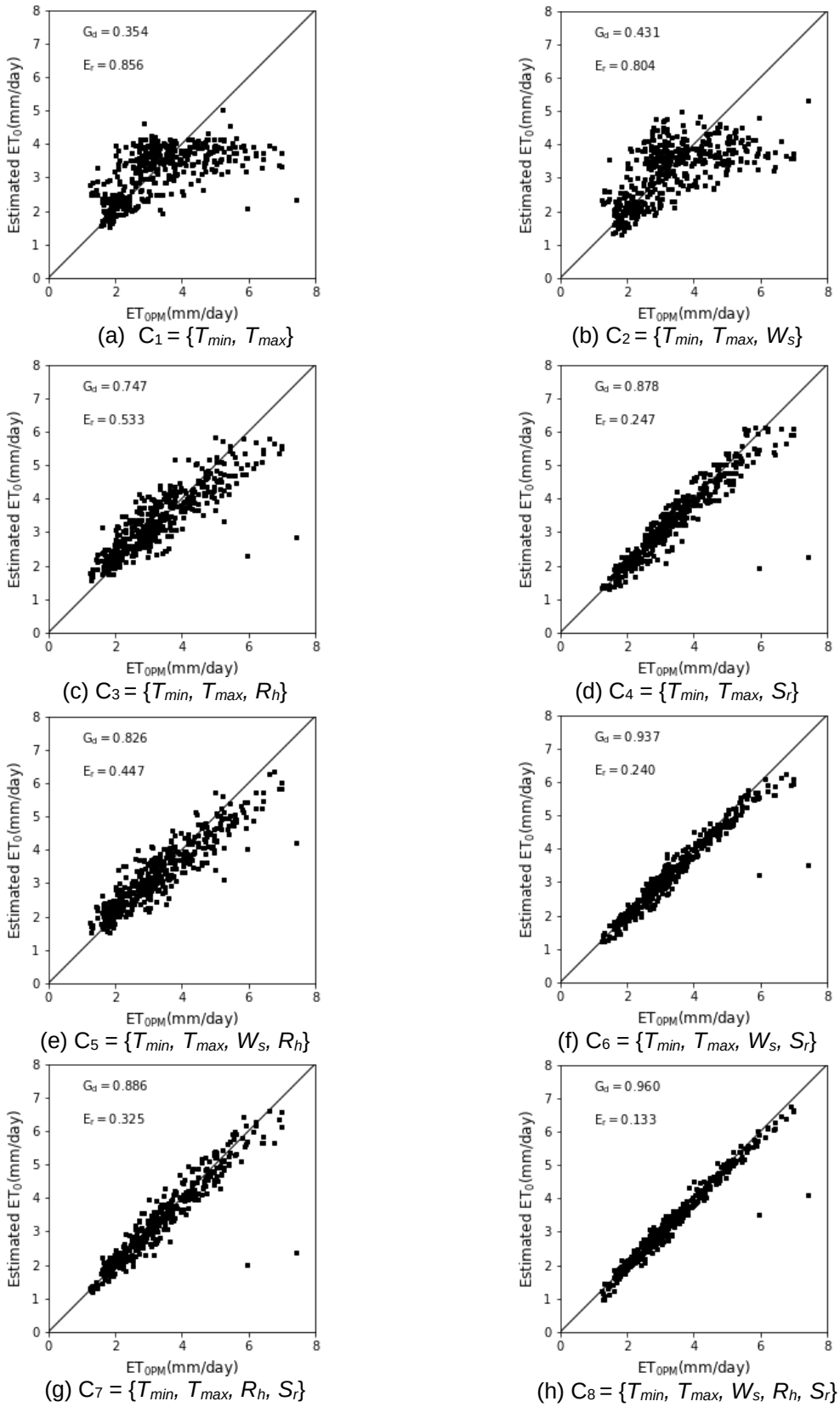

Figure 7. Scatter plots for eight combinations of inputs for Cooch Behar. The scatter plot analysis of g. 7., indicates that the estimated ET_0 using the input combinations C_6, C_7, and demonstrate higher accuracy in scenarios with limited data for Cooch Behar.

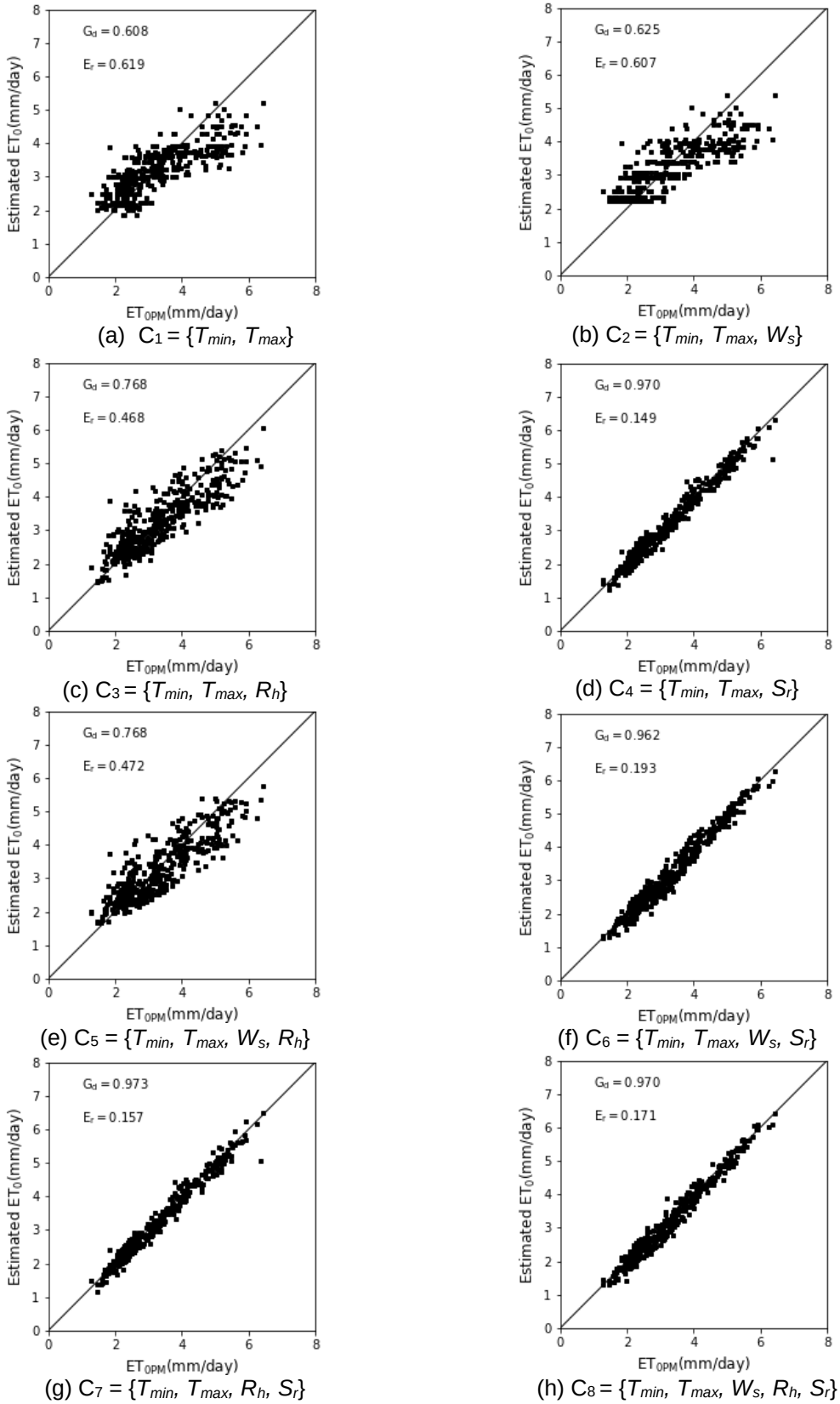

Figure 8. Scatter plots for eight combinations of inputs for Malda. The scatter plot analysis of Fire 8., indicates that the estimated ET_0 using the input combinations C_4, C_7, and demonstrate higher predictive accuracy at Malda.

Table 7. Best models for each of the input combinations at three study locations

	Input Combinations	Best Model	G_d	E_r
Jalpaiguri	C_1	XGB+WOA	0.418	0.751
	C_2	GBM+WOA	0.511	0.680
	C_3	XGB+WOA	0.528	0.659
	C_4	XGB+GWO	0.910	0.281
	C_5	XGB+WOA	0.608	0.600
	C_6	GBM+SFO	0.969	0.167
	C_7	XGB+GWO	0.901	0.292
	C_8	GBM+WOA	0.974	0.152
Cooch Behar	C_1	CAT+SSO	0.354	0.856
	C_2	GBM+GWO	0.431	0.804
	C_3	LGB+SFO	0.747	0.533
	C_4	CAT+SFO	0.878	0.247
	C_5	XGB+GWO	0.826	0.447
	C_6	GBM+SFO	0.937	0.240
	C_7	CAT+GWO	0.886	0.325
	C_8	CAT+SFO	0.960	0.133
Malda	C_1	XGB+GWO	0.608	0.619
	C_2	LGB+SSO	0.625	0.607
	C_3	XGB+WOA	0.768	0.468
	C_4	CAT+SSO	0.970	0.149
	C_5	CAT+WOA	0.768	0.472
	C_6	CAT+SSO	0.962	0.193
	C_7	CAT+WOA	0.973	0.157
	C_8	CAT+GWO	0.970	0.171

For the study location Malda, as an exception, the GBM primary learner (with G_{avg} = 0.822 and E_{avg} = 0.360) outperformed its other optimized versions with (G_{avg} ranging from 0.803 to 0.817 and E_{avg} ranging from 0.365 to 0.374), as projected in Figure 5(a). Figure 5(b) depicts that all the optimized versions of LGB dominated the primary learner LGB (with G_{avg} = 0.810 and E_{avg} = 0.372). The LGB coupled with GWO (LGB+GWO) was the best performer (G_{avg} = 0.822 and E_{avg} = 0.361). Figure 5(c) shows that the XGB primary learner coupled with whale optimizer (XGB+WOA) produced superior results (with G_{avg} = 0.822 and E_{avg} = 0.358) than the primary learner (with G_{avg} = 0.777 and E_{avg} = 0.402). Compared to the other optimized versions, the CAT primary learner performed worse in terms of G_{avg} (= 0.803) and E_{avg} (= 0.377). This observation is very identical to those obtained for the other two locations. Figure 5 (d) depicts that the CAT+SSO is the best learner for Malda (with G_{avg} = 0.826 and E_{avg} = 0.354).

A minor change in estimation accuracy was observed when wind speed (W_s) was incorporated with T_{min} and T_{max} in input combination C_2, the estimation accuracy somewhat improved (with R^2 ranging from 0.431 to 0.625, *NSE* ranging from 0.431 to 0.625, *RMSE* ranging from 0.673 to 0.922 and, *MAE* ranging from 0.541 to 0.685). However, when the W_s in C_{were}as replaced with the fourth parameter relative humidity (R_h), that is, combination C_3, a further improvement of the estimation accuracy was observed (with R^2 ranging from 0.528 to 0.768, *NSE* ranging from 0.528 to 0.768, *RMSE* ranging from 0.529 to 0.743 and, *MAE* ranging from 0.407 to 0.574).

When the fifth input parameter, solar radiation (S_r), was considered along with T_{min} and T_{max} (combination C_4), the estimation accuracy was improved significantly (with R^2 ranging from 0.878 to 0.970, *NSE* ranging from 0.878 to 0.970, *RMSE* ranging from 0.192 to 0.426 and, *MAE* ranging from 0.149 to 0.247).

An addition of another parameter, either W_s or R_h, with combination C_4 (i.e., combinations C_6 and C_7) did not project any further improvement of estimation accuracy over C_4 (with R^2 ranging from 0.886 to 0.973, *NSE* ranging from 0.886 to 0.973, *RMSE* ranging from 0.180 to 0.412 and, *MAE* ranging from 0.134 to 0.237).

When all the five parameters were available (combination C_8) the highest estimation accuracy was achieved at Jalpaiguri and Cooch Behar (with R^2 ranging from 0.925 to 0.974, *NSE* ranging from 0.925 to 0.974, *RMSE* ranging from 0.175 to 0.335 and, *MAE* ranging from 0.129 to 0.159). However, as an exception, the input combination C_7 (Figure. 8(g)) provides the most accurate estimation at Malda.

Another interesting observation is that if the input parameter solar radiation (S_r) was not available along with the other four input parameters (combination C_5), the estimation accuracy dropped significantly (with R^2 ranging from 0.608 to 0.826, *NSE* ranging from 0.608 to 0.826, *RMSE* ranging from 0.510 to 0.677 and, *MAE* ranging from 0.384 to 0.524). It is evident from the experimental results that the input parameter solar radiation (S_r) plays a significant role in the estimation of ET_0 in the North Bengal region of India.

Although the input combination C_8 (C_7 in the case of Malda) provides the highest estimation accuracy of ET_0, the combinations C_4, C_6, and C_7 can also be used for an acceptable accuracy when the complete set of parameters are unavailable, or some input data are missing.

4. Conclusion

Different ET_0 estimation models are required for different location-specific data-limited scenarios. This work suggests a novel architecture for designing an advanced unified model for the precise estimation of ET_0 irrespective of the locations and the available meteorological data. The model was designed using an assembly of the most promising learner-optimizer pairs. As the best-performing learner-optimizer pair is automatically selected from an assembly of learners based on their comparative performances, the estimation of ET_0 with highest precision is always guaranteed. The soil scientists become free from the burden of designing a custom-made model on their own through time-consuming trial-and-error methods. For ET_0, no universal model has been suggested so far. This work provides an elegant solution to this problem by suggesting a general model for ET_0 estimation in diverse data-limited climatic regions without any further customization.

To achieve the goal of better accuracy, the primary learners and their optimized versions were compared under limited and full dataset conditions. It was found that in most cases, the optimized versions had an encouraging effect on performance. The goal of boosting the accuracy of primary learners using hyperparameter optimization was attained in 92% of cases.

Our future attempt is to deploy the proposed model in a cloud-based platform for estimating ET_0 using region-specific meteorological data for better irrigation scheduling. This proposed system will be highly beneficial for irrigation related decision making by the farmers of water- stressed areas.

References

[1] D. Petković, M. Gocic, S. Trajkovic, S. Shamshirband, S. Motamedi, R. Hashim, H. Bonakdari. Determination of the most influential weather parameters on reference evapotranspiration by adaptive neuro-fuzzy methodology. Computers and Electronics in Agriculture, 114, (2015) 277–284. https://doi.org/10.1016/j.compag.2015.04.012

[2] N. Shan, Z. Shi, X. Yang, J. Gao, D. Cai. Spatiotemporal trends of reference evapotranspiration and its driving factors in the Beijing–Tianjin Sand Source Control Project Region, China. Agricultural and Forest Meteorology, 200, (2014) 322–333. https://doi.org/10.1016/j.agrformet.2014.10.008

[3] T. Wu, W. Zhang, X. Jiao, W. Guo, Y.A. Hamoud. Comparison of five Boosting-based models for estimating daily reference evapotranspiration with limited meteorological variables. PLoS ONE, 15(6), (2020) e0235324. https://doi.org/10.1371/journal.pone.0235324

[4] M. Nazari, M.R. Chaichi, H. Kamel, M. Grismer, S.M.M. Sadeghi. (2020). Evaluation of estimation methods for monthly reference evapotranspiration in arid climates. Arid Ecosystems, 10(4), 329–336. https://doi.org/10.1134/S2079096120040150

[5] G.H. Hargreaves, Z.A. Samani. Reference Crop Evapotranspiration from Temperature. Applied Engineering in Agriculture, 1(2), (1985) 96–99. https://doi.org/10.13031/2013.26773

[6] C.H.B. Priestley, R.J. Taylor. On the Assessment of Surface Heat Flux and Evaporation Using Large-Scale Parameters. Monthly Weather Review, 100(2), (1972) 81–92. https://doi.org/10.1175/1520-0493(1972)100%3C0081:OTAOSH%3E2.3.CO;2

[7] S. Irmak, A. Irmak, R.G. Allen, J.W. Jones. Solar and net radiation-based equations to estimate reference evapotranspiration in humid climates. Journal of irrigation and drainage engineering, 129(5), (2003) 336-347. https://doi.org/10.1061/(ASCE)0733-9437(2003)129:5(336)

[8] G.F. Makkink. Testing the Penman formula by means of lysimeters. Journal of the Institution of Water Engineers, 11, (1957) 277–288. https://www.fao.org/3/x0490e/x0490e00.htm

[9] R.G. Allen, L.S. Pereira, D. Raes, M. Smith. Crop evapotranspiration-Guidelines for computing crop water requirements-FAO Irrigation and drainage paper 56. FAO, Rome, 300(9), (1998) D05109. https://www.fao.org/3/x0490e/x0490e00.htm

[10] M. Valipour, M.A.G. Sefidkouhi, M. Raeini-Sarjaz. Spatiotemporal analysis of reference evapotranspiration in arid, semiarid, Mediterranean and very humid climates considering developed models and lysimeter measurements. Water Conservation Science and Engineering, 5(1–2), (2020) 81–96. https://doi.org/10.1007/s41101-020-00087-5

[11] A. Sarma, K. Bharadwaj. Determination of crop-coefficients and estimation of evapotranspiration of

rapeseed using lysimeter and different reference evapotranspiration models. Journal of Agrometeorology, 22(2), (2020) 172-178. https://doi.org/10.54386/jam.v22i2.158

[12] Y. Feng, N. Cui, D. Gong, Q. Zhang, L. Zhao. Evaluation of random forests and generalized regression neural networks for daily reference evapotranspiration modelling. Agricultural Water Management, 193, (2017) 163–173. https://doi.org/10.1016/j.agwat.2017.08.003

[13] Y. Feng, Y. Peng, N. Cui, D. Gong, K. Zhang, Modeling reference evapotranspiration using extreme learning machine and generalized regression neural network only with temperature data. Computers and Electronics in Agriculture, 136, (2017) 71–78. https://doi.org/10.1016/j.compag.2017.01.027

[14] O. Kisi, (2013). Comparison of different empirical methods for estimating daily reference evapotranspiration in Mediterranean climate. Journal of Irrigation and Drainage Engineering, 140(1), 04013002. https://doi.org/10.1061/(ASCE)IR.1943-4774.0000664

[15] W. Jing, Z.M. Yaseen, S. Shahid, M.K. Saggi, H. Tao, O. Kisi, S.Q. Salih, N. Al-Ansari, K. Chau. Implementation of evolutionary computing models for reference evapotranspiration modeling: short review, assessment and possible future research directions. Engineering Applications of Computational Fluid Mechanics, 13(1), (2019) 811–823. https://doi.org/10.1080/19942060.2019.1645045

[16] H. Tabari, P.H. Talaee. Local calibration of the Hargreaves and Priestley-Taylor equations for estimating reference evapotranspiration in arid and cold climates of Iran based on the Penman-Monteith model. Journal of Hydrologic Engineering, 16(10), (2011) 837–845. https://doi.org/10.1061/(ASCE)HE.1943-5584.0000366

[17] Z. Zhou, L. Zhao, A. Lin, W. Qin, Y. Lu, J. Li, Y. Zhong, L. He. Exploring the potential of deep factorization machine and various gradient boosting models in modeling daily reference evapotranspiration in China. Arabian Journal of Geosciences, 13(24), (2020) 1287. https://doi.org/10.1007/s12517-020-06293-8

[18] L. Wang, O. Kisi, B. Hu, M. Bilal, M. Zounemat-Kermani, H. Li. Evaporation modelling using different machine learning techniques. International Journal of Climatology, 37(S1), (2017) 1076–1092. https://doi.org/10.1002/joc.5064

[19] L. Wang, O. Kisi, M. Zounemat-Kermani, H. Li. Pan evaporation modeling using six different heuristic computing methods in different climates of China. Journal of Hydrology, 544, (2016) 407–427. https://doi.org/10.1016/j.jhydrol.2016.11.059

[20] Y. Huang, Y. Lan, S.J. Thomson, A. Fang, W.C. Hoffmann, R.E. Lacey. Development of soft computing and applications in agricultural and biological engineering. Computers and Electronics in Agriculture, 71(2), (2010) 107–127. https://doi.org/10.1016/j.compag.2010.01.001

[21] A. Raza, Y. Hu, M. Shoaib, M.K.A. Elnabi, M. Zubair, M. Nauman, N. Syed. A Systematic Review on Estimation of Reference Evapotranspiration under Prisma Guidelines. Polish Journal of Environmental Studies. 30(6), (2021) 5413-5422. https://doi.org/10.15244/pjoes/136348

[22] M.Y. Chia, Y.F. Huang, C.H. Koo, K.F. Fung. Recent Advances in Evapotranspiration Estimation Using Artificial Intelligence Approaches with a Focus on Hybridization Techniques—A Review. Agronomy, 10(1), (2020) 101. https://doi.org/10.3390/agronomy10010101

[23] N.L.O. Odhiambo, N.R.E. Yoder, N.D.C. Yoder, N.J.W. Hines. Optimization of fuzzy evapotranspiration model through neural training with input–output examples. Transactions of the ASAE, 44(6), (2001) 1625–1633. https://doi.org/10.13031/2013.7049

[24] N.P.N. Balve, N.J.N. Patel. Prediction of evapotranspiration using Fuzzy logic. Journal of Agrometeorology, 18(2), (2016) 311–314. https://doi.org/10.54386/jam.v18i2.958

[25] S. Walls, A.D. Binns, J. Levison, S. MacRitchie. (2020). Prediction of actual evapotranspiration by artificial neural network models using data from a Bowen ratio energy balance station. Neural Computing and Applications, 32(17), 14001–14018. https://doi.org/10.1007/s00521-020-04800-2

[26] S. Dimitriadou, K.G. Nikolakopoulos. Artificial neural networks for the prediction of the reference evapotranspiration of the Peloponnese Peninsula, Greece. Water, 14(13), (2022) 2027. https://doi.org/10.3390/w14132027

[27] P.S. Käfer, N.S. Da Rocha, L.R. Diaz, E.A. Kaiser, D.C. Santos, G.P. Veeck, D.R. Robérti, S.B.A. Rolim, G.G. De Oliveira. Artificial neural networks model based on remote sensing to retrieve evapotranspiration over the Brazilian Pampa. Journal of Applied Remote Sensing, 14(03), (2020) 038504. https://doi.org/10.1117/1.JRS.14.038504

[28] G.M. Mulualem, Y. Liou. Application of artificial neural networks in forecasting a standardized precipitation evapotranspiration index for the Upper Blue Nile Basin. Water, 12(3), (2020) 643. https://doi.org/10.3390/w12030643

[29] A. Raza, M. Shoaib, A. Khan, F. Baig, M.A. Faiz, M.M. Khan, Application of non-conventional soft computing approaches for estimation of reference evapotranspiration in various climatic regions. Theoretical and Applied Climatology, 139(3–4), (2019) 1459–1477. https://doi.org/10.1007/s00704-019-03007-3

[30] E.H. Chouaib, B. Salwa, K. Saïd, C. Abdelghani. Early estimation of daily reference evapotranspiration using machine learning techniques for efficient management of irrigation water. Journal of Physics Conference Series, 2224(1), (2022) 012006. https://doi.org/10.1088/1742-6596/2224/1/012006

[31] F. Granata, R. Gargano, G. De Marinis. Artificial intelligence based approaches to evaluate actual evapotranspiration in wetlands. The Science of the Total Environment, 703, (2019) 135653. https://doi.org/10.1016/j.scitotenv.2019.135653

[32] A. Ayaz, M. Rajesh, S.K. Singh, S. Rehana. Estimation of reference evapotranspiration using machine learning models with limited data. AIMS Geosciences, 7(3), (2021) 268–290. https://doi.org/10.3934/geosci.2021016

[33] L. Wu, Y. Peng, J. Fan, Y. Wang, Y. (2019). Machine learning models for the estimation of monthly mean daily reference evapotranspiration based on cross-station and synthetic data. Hydrology Research, 50(6), 1730–1750. https://doi.org/10.2166/nh.2019.060

[34] J. Fan, W. Yue, L. Wu, F. Zhang, H. Cai, X. Wang, X. Lu, Y. Xiang. Evaluation of SVM, ELM and four tree-based ensemble models for predicting daily reference evapotranspiration using limited meteorological data in different climates of China. Agricultural and Forest Meteorology, 263, (2018) 225–241. https://doi.org/10.1016/j.agrformet.2018.08.019

[35] B. Petković, D. Petković, B. Kuzman, M. Milovančević, K. Wakil, L.S. Ho, K. Jermsittiparsert. Neuro-fuzzy estimation of reference crop evapotranspiration by neuro fuzzy logic based on weather conditions. Computers and Electronics in Agriculture, 173, (2020) 105358. https://doi.org/10.1016/j.compag.2020.105358

[36] R.T.G. Del Cerro, M. Subathra, N.M. Kumar, S. Verrastro, S.T. George. Modelling the daily reference evapotranspiration in semi-arid region of South India: A case study comparing ANFIS and empirical models. Information Processing in Agriculture, 8(1), (2020) 173–184. https://doi.org/10.1016/j.inpa.2020.02.003

[37] M.M. Reis, A.J. Da Silva, J. Zullo, L.D.T. Junior, Santos, A.M. Azevedo, E.M.G. Lopes. Empirical and learning machine approaches to estimating reference evapotranspiration based on temperature data. Computers and Electronics in Agriculture, 165, (2019) 104937. https://doi.org/10.1016/j.compag.2019.104937

[38] J. Shiri, A.H. Nazemi, A.A. Sadraddini, P. Marti, A.F. Fard, O. Kisi, G. Landeras. Alternative heuristics equations to the Priestley–Taylor approach: assessing reference evapotranspiration estimation. Theoretical and Applied Climatology, 138(1–2), (2019) 831–848. https://doi.org/10.1007/s00704-019-02852-6

[39] L.B. Ferreira, F.F. Da Cunha, R.A. De Oliveira, E.I.F. Filho. Estimation of reference evapotranspiration in Brazil with limited meteorological data using ANN and SVM – A new approach. Journal of Hydrology, 572, (2019) 556–570. https://doi.org/10.1016/j.jhydrol.2019.03.028

[40] B. Keshtegar, O. Kisi, M. Zounemat-Kermani, Polynomial chaos expansion and response surface method for nonlinear modelling of reference evapotranspiration. Hydrological Sciences Journal, 64(6), (2019) 720–730. https://doi.org/10.1080/02626667.2019.1601727

[41] V. Nourani, G. Elkiran, J. Abdullahi. Multi-station artificial intelligence based ensemble modeling of reference evapotranspiration using pan evaporation measurements. Journal of Hydrology, 577, (2019) 123958. https://doi.org/10.1016/j.jhydrol.2019.123958

[42] S. Hou, F. Hua, W. Lv, Z. Wang, Y. Liu, G. Wang. Hybrid modeling of flotation height in air flotation oven based on selective bagging ensemble method. Mathematical Problems in Engineering, 2013, (2013) 1–9. https://doi.org/10.1155/2013/281523

[43] M. Guermoui, S. Benkaciali, K. Gairaa, K. Bouchouicha, T. Boulmaiz, J.W. Boland. A novel ensemble learning approach for hourly global solar radiation forecasting. Neural Computing and Applications, 34(4), (2021) 2983–3005. https://doi.org/10.1007/s00521-021-06421-9

[44] A. Bijlwan, S. Pokhriyal, R. Ranjan, R.K. Singh, A. Jha. Machine learning methods for estimating reference evapotranspiration. Journal of Agrometeorology, 26(1), (2024) 63–68. https://doi.org/10.54386/jam.v26i1.2462

[45] D. Yang, S. Yang, J. Huang, S. Zhang, S. Zhang, J. Zhang, Y. Bai. Improving time upscaling of instantaneous evapotranspiration based on machine learning models. Big Earth Data, 9(1), (2024) 127–154. https://doi.org/10.1080/20964471.2024.2423431

[46] P. Guo, J. Cao, J. Lin. Establishment of a reference evapotranspiration-forecasting model based on machine learning. Agronomy, 14(5), (2024) 939. https://doi.org/10.3390/agronomy14050939

[47] Y. Zhao, H. Dong, W. Huang, S. He, C. Zhang. Seamless terrestrial evapotranspiration estimation by machine learning models across the Contiguous United States. Ecological Indicators, 165, (2024) 112203. https://doi.org/10.1016/j.ecolind.2024.112203

[48] A. Ahmadi, M.H. Kazemi, A. Daccache, R.L. Snyder. SolarET: A generalizable machine learning approach to estimate reference evapotranspiration from solar radiation. Agricultural Water Management, 295, (2024) 108779. https://doi.org/10.1016/j.agwat.2024.108779

[49] Y. Zhang, Z. Zhao, J. Zheng. CatBoost: A new

approach for estimating daily reference crop evapotranspiration in arid and semi-arid regions of Northern China. Journal of Hydrology, 588, (2020) 125087. https://doi.org/10.1016/j.jhydrol.2020.125087

[50] J.N. Van Rijn, F. Hutter. Hyperparameter importance across datasets. In Proceedings of the 24th ACM SIGKDD international conference on knowledge discovery & data mining (2018) 2367-2376. https://doi.org/10.1145/3219819.3220058

[51] P. Probst, M.V. Wright, A. Boulesteix. Hyperparameters and tuning strategies for random forest. Wiley Interdisciplinary Reviews Data Mining and Knowledge Discovery, 9, (2019) e1301. https://doi.org/10.1002/widm.1301

[52] R. Khalid, N. Javaid. A survey on hyperparameters optimization algorithms of forecasting models in smart grid. Sustainable Cities and Society, 61, (2020) 102275. https://doi.org/10.1016/j.scs.2020.102275

[53] D. Molina, J. Poyatos, J. Del Ser, S. García, A. Hussain, F. Herrera. Comprehensive Taxonomies of nature- and bio-inspired optimization: Inspiration versus Algorithmic Behavior, Critical Analysis Recommendations. Cognitive Computation, 12(5), (2020) 897–939. https://doi.org/10.1007/s12559-020-09730-8

[54] S. Mirjalili, S.M. Mirjalili, A. Lewis. Grey Wolf Optimizer. Advances in Engineering Software, 69, (2014) 46–61. https://doi.org/10.1016/j.advengsoft.2013.12.007

[55] S. Shadravan, H. Naji, V. Bardsiri. The Sailfish Optimizer: A novel nature-inspired metaheuristic algorithm for solving constrained engineering optimization problems. Engineering Applications of Artificial Intelligence, 80, (2019) 20–34. https://doi.org/10.1016/j.engappai.2019.01.001

[56] S. Mirjalili, A.H. Gandomi, S.Z. Mirjalili, S. Saremi, H. Faris, S.M. Mirjalili. Salp Swarm Algorithm: A bio-inspired optimizer for engineering design problems. Advances in Engineering Software, 114, (2017) 163–191. https://doi.org/10.1016/j.advengsoft.2017.07.002

[57] S. Mirjalili, A. Lewis. The whale Optimization Algorithm. Advances in Engineering Software, 95, (2016) 51–67. https://doi.org/10.1016/j.advengsoft.2016.01.008

[58] H. Li, X. Liu, Z. Huang, C. Zeng, P. Zou, Z. Chu, J. Yi. Newly emerging Nature-Inspired optimization - algorithm review, unified framework, evaluation, and behavioural parameter optimization. IEEE Access, 8, (2020) 72620–72649. https://doi.org/10.1109/ACCESS.2020.2987689

[59] V.H. Quej, C. De La Cruz Castillo, J. Almorox, B. Rivera-Hernandez. Evaluation of artificial intelligence models for daily prediction of reference evapotranspiration using temperature, rainfall and relative humidity in a warm sub-humid environment. Italian Journal of Agrometeorology, 1, (2022) 49–63. https://doi.org/10.36253/ijam-1373

[60] A. Adib, S.S.O. Kalantarzadeh, M.M. Shoushtari, M. Lotfirad, A. Liaghat, M. Oulapour. (2023). Sensitive analysis of meteorological data and selecting appropriate machine learning model for estimation of reference evapotranspiration. Applied Water Science, 13, 83. https://doi.org/10.1007/s13201-023-01895-5

[61] M.E. Akiner, M. Ghasri. Comparative assessment of deep belief network and hybrid adaptive neuro-fuzzy inference system model based on a meta-heuristic optimization algorithm for precise predictions of the potential evapotranspiration. Environmental Science and Pollution Research, 31(30), (2024) 42719–42749. https://doi.org/10.1007/s11356-024-33987-3

[62] H. Tao, L. Diop, A. Bodian, K. Djaman, P.M. Ndiaye, Z.M. Yaseen. Reference evapotranspiration prediction using hybridized fuzzy model with firefly algorithm: Regional case study in Burkina Faso. Agricultural Water Management, 208, (2018) 140–151. https://doi.org/10.1016/j.agwat.2018.06.018

[63] L. Zhao, Y. Wang, Y. Shi, X. Zhao, N. Cui, S. Zhang. Selecting essential factors for predicting reference crop evapotranspiration through tree-based machine learning and Bayesian optimization. Theoretical and Applied Climatology, 155(4), (2023) 2953–2972. https://doi.org/10.1007/s00704-023-04760-2

[64] A. Elbeltagi, O.M. Katipoğlu, V. Kartal, A.D. Mehr, S. Berhail, E.A. Elsadek. Advanced reference crop evapotranspiration prediction: a novel framework combining neural nets, bee optimization algorithm, and mode decomposition. Applied Water Science, 14, (2024) 256. https://doi.org/10.1007/s13201-024-02308-x

[65] Y. Han, J. Wu, B. Zhai, Y. Pan, G. Huang, L. Wu, W. Zeng. Coupling a Bat Algorithm with XGBoost to Estimate Reference Evapotranspiration in the Arid and Semiarid Regions of China. Advances in Meteorology, 2019, (2019) 1–16. https://doi.org/10.1155/2019/9575782

[66] S. Yan, L. Wu, J. Fan, F. Zhang, Y. Zou, Y. Wu. A novel hybrid WOA-XGB model for estimating daily reference evapotranspiration using local and external meteorological data: Applications in arid and humid regions of China. Agricultural Water Management, 244, (2020) 106594. https://doi.org/10.1016/j.agwat.2020.106594

[67] D. Wolpert, W. Macready. No free lunch theorems for optimization. IEEE Transactions on Evolutionary Computation, 1(1), (1997) 67–82. https://doi.org/10.1109/4235.585893

[68] W. Khan, M. Jamshed, S. Fatima. Contribution of agriculture in economic growth: A case study of West Bengal (India). Journal of Public Affairs, 20, (2019) e2031. https://doi.org/10.1002/pa.2031

[69] S. Sahoo, S. Chakraborty, Q.B. Pham, E. Sharifi, S.S. Sammen, M. Vojtek, J. Vojteková, I. Elkhrachy, R. Costache, N.T.T. Linh. Recognition of district-wise groundwater stress zones using the GLDAS-2 catchment land surface model during lean season in the Indian state of West Bengal. Acta Geophysica, 69(1), (2021) 175–198. https://doi.org/10.1007/s11600-020-00509-x

[70] A. Géron. (2017) Hands-on Machine Learning with Scikit-Learn and TensorFlow, O'Reilly Media, USA.

[71] P. Dangeti, P. (2017) Statistics for Machine Learning, Packt Publishing Ltd.

[72] J.H. Friedman. Greedy function approximation: a gradient boosting machine. Annals of statistics, (2001) 1189-1232. https://doi.org/10.1214/aos/1013203451

[73] T. Chen, C. Guestrin. Xgboost: A scalable tree boosting system. In Proceedings of the 22nd acm sigkdd international conference on knowledge discovery and data mining, (2016) 785-794. https://doi.org/10.1145/2939672.2939785

[74] G. Ke, Q. Meng, T. Finley, T. Wang, W. Chen, W. Ma, Q. Ye, T.Y. Liu. (2017). Lightgbm: A highly efficient gradient boosting decision tree. Advances in neural information processing systems, 30.

[75] L. Prokhorenkova, G. Gusev, A. Vorobev, A.V. Dorogush, A. Gulin. CatBoost: unbiased boosting with categorical features. Advances in neural information processing systems, (2018) 31.

[76] V.K. Ayyadevara. Pro Machine Learning Algorithms, Apress: Berkeley, CA, USA, (2018) 283-297.

[77] A.A. Taha, S.J. Malebary. An intelligent approach to credit card fraud detection using an optimized light gradient boosting machine. IEEE Access, 8, (2020) 25579–25587. https://doi.org/10.1109/ACCESS.2020.2971354

[78] Y. Wei, Z. Xing, C. Jian, W. Kangda, W. Shifan, K. Chiam. Use of tree-based machine learning methods for stratigraphic classification in 3D geological modelling, IOP Conference Series: Earth and Environmental Science, 861(7), (2021) 072039. https://doi.org/10.1088/1755-1315/861/7/072039

[79] J. Nayak, B. Naik, P.B. Dash, A. Souri, V. Shanmuganathan. Hyper-parameter tuned light gradient boosting machine using memetic firefly algorithm for hand gesture recognition. Applied Soft Computing, 107, (2021) 107478. https://doi.org/10.1016/j.asoc.2021.107478

[80] N. Ngo, T.T.H. Truong, N. Truong, A. Pham, N. Huynh, T.M. Pham, V.H.S. Pham. Proposing a hybrid metaheuristic optimization algorithm and machine learning model for energy use forecast in non-residential buildings. Scientific Reports, 12, (2022) 1065. https://doi.org/10.1038/s41598-022-04923-7

[81] D. Markovics, M.J. Mayer. Comparison of machine learning methods for photovoltaic power forecasting based on numerical weather prediction. Renewable and Sustainable Energy Reviews, 161, (2022) 112364. https://doi.org/10.1016/j.rser.2022.112364

[82] L. Yin, F. Tao, Y. Chen, F. Liu, J. Hu. Improving terrestrial evapotranspiration estimation across China during 2000–2018 with machine learning methods. Journal of Hydrology, 600, (2021) 126538. https://doi.org/10.1016/j.jhydrol.2021.126538

[83] D. Althoff, S.H.B. Dias, R. Filgueiras, L.N. Rodrigues. ETO-Brazil: A daily gridded reference evapotranspiration data set for Brazil (2000–2018). Water Resources Research, 56(7), (2020). https://doi.org/10.1029/2020WR027562

[84] T. Dutta, S. Bhattacharyya, S. Dey, J. Platos. Border Collie optimization. IEEE Access, 8, (2020) 109177–109197. https://doi.org/10.1109/ACCESS.2020.2999540

[85] X. Lu, J. Fan, N. LifengWu, J. Dong. Forecasting Multi-Step Ahead Monthly Reference Evapotranspiration Using Hybrid Extreme Gradient Boosting with GreyWolf Optimization Algorithm. Computer Modeling in Engineering & Sciences, 125(2), (2020) 699–723. https://doi.org/10.32604/cmes.2020.011004

Authors Contribution Statement

All authors contributed equally to this work and approved the final version of the manuscript.

Funding

The authors declare that no funds, grants or any other support were received during the preparation of this manuscript.

Competing Interests

The authors declare that there are no conflicts of interest regarding the publication of this manuscript.

Data Availability

The data supporting the findings of this study can be obtained from the corresponding author upon reasonable request.

Has this article screened for similarity?

Yes

About the License